American Mineralogist, Volume 76, pages 1836–1856, 1991

The crystal chemistry of the milarite-group minerals

Frank C. Hawthorne, Mitsuyoshi Kimata,* Petr Černý, Neil Ball
Department of Geological Sciences, University of Manitoba, Winnipeg, Manitoba R3T 2N2, Canada

George R. Rossman
Division of Geological and Planetary Sciences, California Institute of Technology, Pasadena, California 91125, U.S.A.

Joel D. Grice
Mineral Sciences Division, Canadian Museum of Nature, Ottawa, Ontario K1P 6P4, Canada

Abstract

The crystal structures of six natural milarites ($A_2B_2C[T2_3T1_{12}O_{30}](H_2O)_x$, $P6/mcc$, $a \sim 10.40$, $c \sim 13.80$ Å, $Z = 2$) covering the range of known compositions have been refined to R indices of ~3% using Mo$K\alpha$ X-ray intensity data. Previously proposed split-atom models for the A and B sites are confirmed. Polarized spectroscopy in the infrared region shows H_2O to be the only significant H-bearing group. Band polarization characteristics show the H-H vector to be $\perp \mathbf{c}$ and the H_2O plane to be $\| \mathbf{c}$; this corresponds to the type II H_2O found in the related structures of beryl and cordierite. There is a quantitative correlation between band intensity and H_2O content, and the observed molar absorptivities are similar to those measured in cordierite.

Milarite has a beryllo-alumino-silicate framework structure. The framework is a four-connected three-dimensional net, one of a series of seven simple nets with prominent double rings of tetrahedra previously derived by Hawthorne and Smith (1986). There are 15 minerals with this net as the basic tetrahedral arrangement; in general, Si is strongly to completely ordered into the ring tetrahedra, and the other tetrahedral cations (Li, Be, B, Al, Mg, Fe^{2+}, Fe^{3+}, Mn^{2+}, and Zn) are strongly to completely ordered into the ring-linking tetrahedra. The important substitution in normal milarite is $Na^{B} + Be^{T2} = \square^{B} + Al^{T2}$ with the amount of Be varying between approximately 1.5 and 2.5 apfu; in (Y,REE)-bearing milarite, the important substitution is $(Y,REE)^{A} + Be^{T2} = Ca^{A} + Al^{T2}$ with the amount of Be varying up to 3.0 atoms pfu. The mean bond lengths of the polyhedra involved in these substitutions vary accordingly, and linear models of this behavior are developed. In addition, there is chemical evidence of a small amount of Al ⇌ Si substitution at the T1 site. Similar linear models are developed for the whole group of milarite-type minerals.

Milarite is found in a variety of environments, from vugs in plutonic rocks through diverse pegmatites to hydrothermal ore deposits and alpine veins; a review of specific parageneses is given. Milarite is a low-temperature hydrothermal mineral crystallizing in the range of 200–250 °C at low pressures. Associated minerals suggest that milarite crystallizes from alkaline fluids with Be being transported as fluor-complexes and carbonate complexes. Other members of the milarite group occur in peralkaline rocks, meteorites, peraluminous volcanic rocks, and high-grade metamorphic rocks, as well as other geochemically more unusual rocks, and form under a wide variety of P-T conditions.

Introduction

Milarite is a framework beryllo-alumino-silicate mineral with the ideal formula $(K,Na)Ca_2[(Be_2Al)Si_{12}O_{30}]\cdot xH_2O$ where $x \sim 3/4$ originally described from Val Giuf, Switzerland (Kuschel, 1877). It is generally found in hydrothermal veins and granitic pegmatites, and it shows significant variations in chemical composition with variation in paragenetic sequence and geographic locality. Milarite is possibly much more common than is generally realized, as it can be mistaken for quartz or apatite in hand specimen. It has been investigated extensively because of its anomalous optical properties, being morphologically hexagonal but often having biaxial optics. It is the prototype mineral for a large structural group that includes osumilite. In the last ten years, it has been recognized that osumilite is much more common than hitherto realized. The crystal-chemical relations of the milarite group have been intensively investigated over the last

* Present address: Institute of Geosciences, University of Tsukuba, Ibaraki 305, Japan.

0003–004X/91/1112–1836$02.00

ten years (Černý et al., 1980; Armbruster et al., 1989; Kimata and Hawthorne, 1989), and a general review and synthesis are warranted.

The milarite structure is extremely flexible from a chemical viewpoint, and a considerable number of minerals (Hawthorne and Smith, 1986) and synthetic compounds (Pushcharovskii et al., 1972; Sandomirskii et al., 1977) adopt this basic atomic arrangement. In particular, it seems to be a structure type that is favored by the light lithophile elements. It is notable that many of the milarite-group minerals have been discovered fairly recently and in a broad spectrum of geological environments. This is probably due to two factors: first, these minerals are easily misidentified both in hand specimen and by powder diffraction; second, the light lithophile elements that are so important in many minerals of this group are easily overlooked in an electron microprobe examination. Milarite itself usually contains 1–2 wt% H_2O. Although the position of H_2O in the structure has been located by diffraction methods, there has hitherto been no spectroscopic examination of the role of H_2O in the milarite structure. In particular, Forbes et al. (1972) suggested that milarite may contain hydronium (H_3O) groups rather than H_2O groups. Obviously this possibility is of great relevance to the polyvalent chemical substitutions operative in the structure. In addition, the complexity of the role of H_2O in the related structures of beryl and cordierite indicates that infrared work on milarite is desirable. In view of the increase in importance of this group in the last few years, we thought it worthwhile to review the previous work done, examine the stereochemical variations across the range of milarite compositions (sensu stricto), and synthesize both the available crystal-chemical and paragenetic information.

Experimental

Sample description

The physical properties and chemical compositions of four of the samples examined here were given by Černý et al. (1980), whereas the other two were only recently reported as a new Y-rich Al-poor variety (Černý et al., 1991). Here we shall retain the sample numbers given by Černý et al. (1980); new samples are numbered 36 and 37.

Sample 25. From Guanajuato, Mexico [National Museum of Natural History (NMNH) no. 121230]; this consists of pale yellow columnar crystals up to 5 × 18 mm in size. These occur as slightly divergent aggregates of hexagonal prisms terminated by basal pinacoids, and they are associated with adularia and minor quartz. Sample NMNH no. 120408 from the same locality was used for the infrared study.

Sample 33. From Tittling, Bavaria (research collection of P. Černý, obtained from C. Tennyson, Technische Universität Berlin); this consists of white to colorless crystals up to 2 × 5 mm in size, with dominant prism, pyramid, and minor basal pinacoid; it is associated with quartz, albite, and chlorite.

Sample 35. From East Siberia, USSR (research collection of P. Černý); this consists of a pale pink aggregate of anhedral columnar crystals up to 3 × 20 mm in size; it is associated with a pale green variety of different composition (Novikova, 1972).

Sample 30. From Rössing, Swakopmund, Namibia (National Museum of Natural History Washington no. C6562); this consists of pale yellow columnar crystals up to 3 × 9 mm in size, with well-developed prismatic and basal pinacoidal faces and minor pyramidal faces. Sample 7935 from the California Institute of Technology collection was also used in the infrared work.

Sample 36. From Jaguaraçú, Brazil (research collection of P. Černý, obtained from R. V. Gaines); this consists of a translucent white columnar crystal 6 × 12 mm in size; the crystal shows prismatic faces and is terminated by a basal pinacoid. Underlying the latter is a ~0.75-mm thick cap of transparent, pale greenish yellow material that proved to be of significantly different (Y,REE)-poor composition.

Sample 37. From Strange Lake, Quebec (CANMET case sample SL258-71); this consists of a pale yellow, clear, hexagonal prism terminated by a minor hexagonal pyramid and basal pinacoid. The crystal was from an 8-mm vug in a coarse-grained quartz-feldspar (predominantly microcline) segregation within the medium-grained granite.

Other samples used in the infrared work are NMNH no. 135779 from the Foote mine, NMNH no. 119156 from Věžná, and NMNH no. B20407 from Val Giuf.

Chemical analysis

Subsequent to the X-ray intensity data measurements, the crystals were detached from their glass fibers, mounted in pyccolyte in a 1-in. plexiglas disk, and ground and polished. Electron microprobe analyses were performed on a Cameca instrument in the wavelength-dispersive mode with an operating voltage of 15 kV and a beam current of 25 nA. A fairly large beam diameter (10 μm) was used to minimize potential sample damage during analysis. Data for standards were obtained for 25 s or 0.25% precision per element, whichever was the more efficient procedure. Standards used were beryl (Al$K\alpha$, Si$K\alpha$), diopside (Ca$K\alpha$), $NaScSi_2O_6$ (Na$K\alpha$), and orthoclase (K$K\alpha$); no other element was observed on ED spectra collected on the same grains. Twenty analyses were obtained on each crystal; the entire crystal was covered in each case in order to give good average analyses. Data reduction was done with a conventional ZAF routine; average analyses are given in Table 1.

X-ray data measurements

Crystals for intensity data measurements were selected on the basis of optical clarity, homogeneity, freedom from inclusions, and equant shape. The crystals were mounted on a Nicolet R3M automated four-circle diffractometer, and 25 intense reflections were centered using graphite-monochromated Mo$K\alpha$ X-radiation. Least-squares re-

TABLE 1. Chemical analyses for milarite samples

	25		33		35	30		36	37
	CHJ*	Probe	CHJ	Probe	CHJ	CHJ	Probe	Probe	Probe
SiO_2	71.35	72.78	70.65	72.96	71.23	71.81	72.85	70.20	67.69
Al_2O_3	5.68	5.84	4.34	4.34	7.02	3.40	3.31	1.50	0.26
BeO	4.58	(4.58)	6.71	(6.71)	4.52	5.07	(5.07)	—	—
BeO_c**	[5.18]	[4.94]	[5.39]	[5.37]	[4.28]	[5.80]	[5.52]	[6.30]	[6.55]
MnO	0.25	0.19	0.00	0.01	0.00	0.15	0.02	0.00	0.06
CaO	11.40	11.17	10.80	11.13	9.32	11.60	11.28	7.70	6.00
Na_2O	0.17	0.08	0.52	0.04	1.90	0.49	0.10	0.15	0.06
K_2O	4.95	4.81	4.97	5.08	4.03	4.52	4.68	4.80	4.64
Rb_2O	(0.03)	0.03	(0.04)	0.04	—	(0.02)	0.02	—	—
BaO	(0.08)	0.08	(0.02)	0.02	—	(0.04)	0.04	—	—
Y_2O_3	(0.01)	0.01	(0.29)	0.29	—	(0.00)	0.00	5.10	6.48
H_2O	1.20	(1.20)	1.29	(1.29)	1.65	1.68	(1.68)	—	—
Sum	99.70	100.77	99.63	100.57	99.67	98.78	99.05	96.91†	94.33‡
Si	11.92	11.98	11.74	11.82	11.86	12.12	12.21	—	—
Al	1.12	1.13	0.85	0.83	1.38	0.68	0.65	—	—
Be	1.84	1.81	2.68	2.61	1.81	2.06	2.04	—	—
Mn	0.04	0.03	0.00	0.00	0.00	0.02	0.00	—	—
Ca	2.04	1.97	1.92	1.93	1.66	2.10	2.03	—	—
Na	0.06	0.03	0.17	0.01	0.61	0.16	0.03	—	—
K	1.06	1.01	1.05	1.05	0.86	0.97	1.00	—	—
Y	0.00	0.00	0.03	0.03	0.00	0.00	0.00	—	—
Sum	18.07	17.97	18.44	18.29	18.18	18.11	17.98	—	—
Si	11.83	11.93	11.95	12.03	11.90	12.00	12.14	12.09	12.13
Al	1.11	1.13	0.87	0.84	1.38	0.67	0.65	0.30	0.05
Be_c	2.06	1.95	2.19	2.13	1.72	2.33	2.21	2.61	2.82
Mn	0.04	0.03	0.00	0.00	0.00	0.02	0.00	0.00	0.01
Ca	2.03	1.96	1.96	1.97	1.67	2.08	2.01	1.42	1.15
Na	0.06	0.03	0.17	0.01	0.62	0.16	0.03	0.05	0.02
K	1.05	1.01	1.07	1.07	0.86	0.96	1.00	1.05	1.06
Y	0.00	0.00	0.03	0.03	0.00	0.00	0.00	0.47	0.62
Sum	18.17	18.03	18.23	18.08	18.15	18.23	18.05	18.05†	18.01‡

Note: 25 = Guanajuato; 33 = Tittling; 35 = east Siberia pink; 30 = Rössing; 36 = Jaguaraçú green; 37 = Strange Lake.
* From Černý et al. (1980).
** BeO calculated such that Si + Al + Be = 15 apfu.
† Includes Yb_2O_3 0.60, Er_2O_3 0.30, Dy_2O_3 0.20 wt%; Yb 0.03; Er 0.02, Dy 0.01 apfu.
‡ Includes Ce_2O_3 0.71, Nd_2O_3 0.44, Er_2O_3 0.57, Dy_2O_3 0.72 wt%; Ce 0.05, Nd 0.03, Er 0.03, Dy 0.04 apfu.

finement of the setting angles produced the (hexagonally constrained) cell dimensions given in Table 2. Reflections were measured to a maximum 2θ angle of 60° according to the experimental procedure of Hawthorne (1985); numbers of reflections are given in Table 2, together with other information pertinent to X-ray data measurement and structure refinement. Ten strong reflections uniformly distributed with regard to 2θ were measured at 10° intervals of ψ from 0 to 350°. These data were used to calculate an ellipsoidal shape for the crystal, which was then used for absorption corrections on the whole intensity data set; azimuthal R indices were of the order of 1.0–1.5% (Table 2). Data were corrected for Lorentz, polarization, and background effects, then averaged and reduced to structure factors. A reflection was classed as observed if its intensity exceeded that of 4 sd based on counting statistics; final numbers of observed reflections are given in Table 2.

Spectroscopic data

Samples for infrared spectroscopy were prepared as thin, doubly polished slabs parallel to [001], following the procedures of Goldman et al. (1977).

Spectra were measured with a combination of Perkin Elmer model 180 (IR), Nicolet 60SX (IR and near IR), and Cary 17I (near IR) spectrophotometers. Spectroscopic measurements were obtained on sample regions from 100 μm to 2 × 4 mm that were as free as possible from inclusions and cracks. In the 3600-cm^{-1} region, samples were ground as thin as 15 μm to obtain on-scale measurements. Low-temperature spectra were measured with the sample attached to a liquid N–cooled cold finger in a vacuum dewar.

Structure refinement

Scattering curves for neutral atoms together with anomalous dispersion corrections were taken from the *International Tables for X-ray Crystallography* (1974). R indices are of the form given in Table 2 and are expressed as percentages. The SHELXTL system of programs (Sheldrick, 1981) was used for the computational procedures.

Refinements were initiated using the atomic positions of milarite from King's Mountain (Černý et al., 1980) together with site occupancies suggested by typical chemical relations of the species concerned. Full-matrix refinement of all variables for an isotropic displacement model converged to R indices of approximately 4.5% (Table 2). Upon conversion to an anisotropic displacement model, the A cation(s) showed exaggerated anisot-

TABLE 2. Miscellaneous data regarding milarite refinements

	25	33	35	30	36	37
a (Å)	10.410(1)	10.404(2)	10.415(3)	10.396(1)	10.342(2)	10.340(1)
c	13.845(3)	13.825(5)	13.763(5)	13.781(4)	13.777(6)	13.758(2)
V (Å^3)	1299.3(5)	1296.0(7)	1293.0(7)	1289.8(5)	1275.8(9)	1273.9(4)
Space group	*P6/mcc*	*P6/mcc*	*P6/mcc*	*P6/mcc*	*P6/mcc*	*P6/mcc*
Z	2	2	2	2	2	2
Crystal Size (mm)	0.20 × 0.24 ×0.36	0.20 × 0.24 ×0.30	0.18 × 0.20 ×0.30	0.14 × 0.16 ×0.18	0.22 × 0.30 ×0.32	0.15 × 0.15 ×0.25
Radiation Mono.	Mo$K\alpha$ graphite	Mo$K\alpha$ graphite	Mo$K\alpha$ graphite	Mo$K\alpha$ graphite	Mo$K\alpha$ graphite	Mo$K\alpha$ graphite
R_{az}%	1.4	1.3	1.3	0.9	1.4	1.0
Total $\|F\|$	1527	1521	1515	1516	1503	1501
No of $\|F_o\|$	629	581	607	555	561	561
R_{iso}%	4.6	4.3	4.5	4.1	4.5	5.6
R_{anis}%	2.9	3.1	3.2	3.4	3.3	4.1

Note: 25 = Guanajuato; 33 = Tittling; 35 = east Siberia pink; 30 = Rössing; 36 = Jaguaraçú green; 37 = Strange Lake.

ropy. This was taken as evidence for significant displacement of the cation off the special position; the electron density was modeled as a split site with an isotropic displacement factor. This gave the same R indices as were obtained for the ordered anisotropic displacement model, but we prefer the split-site model on physical grounds; both models gave consistent results across the series. Full-matrix least-squares refinement of all variables (including site occupancies) converged to the R indices given in Table 2. Final atomic parameters are given in Table 3, and structure factor tables (Table 4) are deposited;[1] selected interatomic distances and angles are given in Table 5.

GENERAL STRUCTURAL RELATIONS

In the Bragg classification of the silicates, milarite is considered as a double-ring structure. However, if the chemical identity of the tetrahedrally coordinated cation is not considered, as suggested by Zoltai (1960) and Liebau (1985), milarite has a tetrahedral framework structure. Smith (1977) instituted a systematic examination of the derivation and characterization of four-connected three-dimensional nets as topological models for framework silicate structures. Hawthorne and Smith (1986) developed a new family of nets based on the insertion of two-connected vertices into alternate edges of two-dimensional three-connected nets combined with the usual out-of-plane operations; the milarite framework is based on one of the resulting nets. This topological approach is of interest here for two reasons: first, the milarite framework is seen as just one of a series of possible atomic arrangements of related topology; second, the relative ordering of tetrahedral cations over the vertices of the nets seems to be related to the local connectivity of the framework. Thus a further examination of the relationships within this family of nets is of interest.

[1] A copy of the structure factor tables (Table 4) may be ordered as Document AM-91-483 from the Business Office, Mineralogical Society of America, 1130 Seventeenth Street, Suite 330, Washington, DC 20036, U.S.A. Please remit $5.00 in advance for the microfiche.

Hawthorne and Smith (1986) developed 46 four-connected three-dimensional nets based on insertion of two-connected vertices into the three-connected two-dimensional nets 6^3, 3.12^2, 4.8^2, and 4.6.12. Hawthorne and Smith (1988) show that one of the topological consequences of developing four-connected three-dimensional nets by out-of-plane linkages between stacks of two-dimensional nets is that the initial three-connected vertices must lie on infinite paths within a single prototype two-dimensional net. Such infinite paths are of two types: open paths (which do not return to their starting vertex) and circuits (closed paths). Thus the family derived by Hawthorne and Smith (1986) can be divided into two types according to the graphical characteristics of the three-connected vertices in the prototype two-dimensional nets: nets with open paths and nets with (infinite) circuits of three-connected vertices. The milarite framework has double six-membered rings of such vertices and is just one of a family of possible structures based on sigma-transformed nets (Shoemaker et al., 1973) containing such double n-membered rings.

The simplest case is net 278, the basis of the beryl structure (Fig. 1, Table 6). Two-connected vertices are inserted into the edges of the plane net 6^3 such that alternate six-membered rings of three-connected vertices are preserved (Fig. 1a). If topologically equivalent nets are stacked orthogonal to the plane of the prototype two-dimensional net such that the (initially) two-connected vertices link to vertically adjacent nets, a four-connected three-dimensional net results. If the six-membered rings of (initially) three-connected vertices contrarotate in adjacent layers, the edges connecting to the (initially) two-connected vertices take on a tetrahedral arrangement (Fig. 1b). The polyhedral representation of this net is essentially the tetrahedral framework of beryl and indialite.

The key topological features of the framework are actually encapsulated in Figure 1a, and for simplicity we will use this type of representation here. All nets with rings of (initially) three-connected vertices are shown in Figure 2, in both cases ordered according to the number of tetrahedra in the n-membered rings; note that there is

TABLE 3. Final atomic parameters* for milarite samples

		25	33	35	30	36	37
A	x	⅓	⅓	⅓	⅓	⅓	⅓
	y	⅔	⅔	⅔	⅔	⅔	⅔
	z	0.2437(4)	0.2410(2)	0.2372(2)	0.2390(2)	0.23572(7)	0.2314(6)
	U_{eq}	189(4)	154(4)	159(5)	141(7)	46(3)	84(12)
B	x	⅓	⅓	⅓	⅓	⅓	⅓
	y	⅔	⅔	⅔	⅔	⅔	⅔
	z	0.0404(19)	0.0349(15)	0.0250(14)	0.0298(18)	0.0499(13)	0.050(1)
	U_{eq}	689(97)	585(77)	645(79)	674(106)	602(62)	267(50)
	U_{11}	685(120)	427(70)	361(32)	548(88)	578(76)	238(55)
	U_{22}	685	427	361	548	578	238
	U_{33}	695(160)	900(185)	1214(227)	927(264)	649(107)	327(104)
	U_{12}	343(60)	213(35)	180(16)	274(44)	289(38)	119(27)
C	x	0	0	0	0	0	0
	y	0	0	0	0	0	0
	z	¼	¼	¼	¼	¼	¼
	U_{eq}	205(4)	190(6)	189(6)	184(8)	193(7)	181(7)
	U_{11}	206(5)	183(7)	186(7)	172(9)	182(9)	172(8)
	U_{22}	206	183	186	172	182	172
	U_{33}	204(8)	204(10)	196(10)	207(15)	216(13)	197(13)
	U_{12}	103(3)	91(4)	93(4)	86(4)	91(4)	86(4)
T1	x	0.08239(6)	0.08168(7)	0.07988(7)	0.0811(1)	0.08132(8)	0.08085(9)
	y	0.33642(7)	0.33625(8)	0.33542(8)	0.3363(1)	0.33844(9)	0.3380(1)
	z	0.11217(4)	0.11257(4)	0.11324(4)	0.1127(1)	0.11249(5)	0.11262(6)
	U_{eq}	94(2)	88(2)	92(2)	81(4)	87(3)	72(3)
	U_{11}	100(3)	87(3)	95(3)	75(4)	77(3)	69(4)
	U_{22}	117(3)	103(3)	112(3)	95(4)	107(3)	95(4)
	U_{33}	67(2)	73(2)	69(3)	74(4)	78(3)	51(4)
	U_{12}	53(2)	47(3)	52(2)	43(4)	47(3)	41(4)
	U_{13}	−5(2)	−3(2)	−6(2)	−5(4)	−4(3)	−2(3)
	U_{23}	−8(2)	−7(2)	−11(3)	−11(4)	−13(3)	−11(4)
T2	x	0	0	0	0	0	0
	y	½	½	½	½	½	½
	z	¼	¼	¼	¼	¼	¼
	U_{eq}	94(7)	90(10)	81(12)	73(17)	97(21)	45(20)
	U_{11}	110(10)	98(15)	80(17)	94(25)	104(30)	58(31)
	U_{22}	101(7)	93(11)	79(14)	48(18)	105(30)	48(21)
	U_{33}	74(9)	81(13)	83(16)	93(24)	83(29)	32(29)
	U_{12}	55(5)	49(7)	40(9)	47(13)	52(15)	29(15)
O1	x	0.0954(3)	0.0946(4)	0.0929(4)	0.0940(6)	0.0946(4)	0.0941(5)
	y	0.3835(3)	0.3830(3)	0.3822(3)	0.3837(5)	0.3873(4)	0.3872(5)
	z	0	0	0	0	0	0
	U_{eq}	194(10)	190(11)	211(12)	200(18)	205(14)	187(15)
	U_{11}	290(13)	298(16)	332(16)	330(26)	319(19)	315(22)
	U_{22}	222(12)	208(13)	234(14)	225(22)	206(16)	203(18)
	U_{33}	71(8)	68(9)	73(10)	67(14)	80(11)	42(14)
	U_{12}	128(11)	129(12)	146(13)	155(21)	123(15)	129(17)
O2	x	0.1957(2)	0.1951(2)	0.1939(2)	0.1949(3)	0.1959(3)	0.1959(3)
	y	0.2761(2)	0.2759(2)	0.2758(2)	0.2759(4)	0.2779(3)	0.2776(3)
	z	0.1342(1)	0.1340(1)	0.1347(1)	0.1342(2)	0.1333(2)	0.1327(2)
	U_{eq}	176(7)	167(7)	185(8)	173(12)	180(9)	162(10)
	U_{11}	178(8)	169(9)	190(9)	159(14)	168(11)	156(13)
	U_{22}	244(9)	230(10)	256(11)	235(16)	244(12)	234(13)
	U_{33}	160(7)	162(8)	172(8)	188(13)	197(10)	175(12)
	U_{12}	146(7)	145(8)	159(9)	146(13)	154(10)	157(11)
	U_{13}	−17(7)	−22(7)	−33(8)	−34(12)	−36(9)	−37(10)
	U_{23}	−29(7)	−24(8)	−45(8)	−46(13)	−52(10)	−44(10)
O3	x	0.1160(2)	0.1154(2)	0.1142(2)	0.1147(3)	0.1158(2)	0.1155(2)
	y	0.4730(2)	0.4729(2)	0.4727(2)	0.4733(3)	0.4751(2)	0.4747(2)
	z	0.1804(1)	0.1804(1)	0.1807(1)	0.1809(2)	0.1821(1)	0.1822(2)
	U_{eq}	128(6)	120(6)	129(6)	108(10)	118(7)	97(8)
	U_{11}	145(7)	131(8)	157(8)	120(12)	118(7)	108(10)
	U_{22}	138(7)	125(8)	132(8)	110(12)	129(10)	112(10)
	U_{33}	104(6)	112(7)	112(7)	98(10)	113(8)	88(10)
	U_{12}	74(6)	70(7)	82(7)	60(10)	65(8)	69(9)
	U_{13}	−3(6)	−6(7)	−2(7)	−6(10)	5(8)	−2(9)
	U_{23}	−28(6)	−24(7)	−30(7)	−23(10)	−28(8)	−27(9)

* $U_{ij} = U_{ij} \times 10^4$.

TABLE 5. Selected interatomic distances (Å) and angles (°) in milarite samples

		25	33	35	30	36	37
A-O3	×3	2.322(1)	2.310(2)	2.299(2)	2.297(2)	2.253(2)	2.327(2)
A-O3a	×3	2.393(1)	2.411(2)	2.441(2)	2.420(3)	2.411(2)	2.327(2)
⟨A-O⟩		2.357	2.361	2.370	2.359	2.332	2.327
O3-O3a	×3	2.617(2)	2.612(3)	2.595(3)	2.585(5)	2.537(4)	2.536(4)
O3-O3b	×3	3.164(2)	3.170(4)	3.180(3)	3.172(4)	3.137(4)	3.135(4)
O3-O3c	×6	3.724(2)	3.729(3)	3.747(4)	3.730(5)	3.686(4)	3.692(4)
⟨O-O⟩A		3.307	3.310	3.312	3.304	3.261	3.264
O3-A-O3a	×3	67.4(1)	67.1(1)	66.3(1)	66.4(1)	65.8(1)	65.5(1)
O3-A-O3b	×3	84.3(1)	84.3(1)	84.2(1)	84.4(1)	84.5(1)	84.1(1)
O3-A-O3c	×3	106.6(1)	107.6(1)	109.2(1)	108.5(1)	109.8(1)	111.3(1)
O3a-A-O3	×3	102.2(1)	101.3(1)	100.3(1)	100.8(1)	99.7(1)	98.3(1)
⟨O-A-O⟩		90.1	90.1	90.0	90.0	90.0	89.8
B-O1	×3	2.799(5)	2.790(4)	2.784(3)	2.774(5)	2.790(5)	2.793(6)
B-O3	×3	2.894(17)	2.946(15)	3.045(13)	2.996(17)	2.801(11)	2.798(14)
⟨B-O⟩		2.847	2.868	2.915	2.870	2.796	2.796
C-O2	×12	3.021(2)	3.017(2)	3.008(2)	3.012(3)	3.021(2)	3.022(2)
T1-O1		1.614(1)	1.616(1)	1.618(1)	1.614(2)	1.614(1)	1.615(2)
T1-O2		1.618(3)	1.617(3)	1.617(3)	1.619(5)	1.619(4)	1.620(4)
T1-O2d		1.621(2)	1.618(2)	1.618(2)	1.616(4)	1.618(4)	1.592(4)
T1-O3		1.593(2)	1.588(2)	1.588(2)	1.593(3)	1.594(2)	1.609(3)
⟨T1-O⟩		1.612	1.610	1.610	1.611	1.611	1.609
O1-O2		2.638(3)	2.633(4)	2..633(4)	2.636(6)	2.633(5)	2.630(5)
O1-O2d		2.654(2)	2.648(3)	2.651(3)	2.648(4)	2.648(3)	2.637(4)
O1-O3		2.636(2)	2.634(2)	2.629(2)	2.632(3)	2.639(2)	2.636(3)
O2-O2d		2.560(1)	2.556(1)	2.555(1)	2.554(1)	2.558(1)	2.555(1)
O2-O3		2.646(3)	2.645(4)	2.645(4)	2.651(6)	2.643(4)	2.646(5)
O2d-O3		2.649(2)	2.652(3)	2.660(3)	2.654(4)	2.658(3)	2.655(3)
⟨O-O⟩T1		2.631	2.628	2.630	2.629	2.630	2.627
O1-T1-O2		109.4(1)	109.0(2)	109.0(2)	109.2(3)	109.1(2)	108.8(2)
O1-T1-O2d		110.3(1)	109.9(1)	110.0(1)	110.1(1)	110.0(1)	109.7(2)
O1-T1-O3		110.6(1)	110.6(1)	110.2(1)	110.3(2)	110.7(2)	110.5(2)
O2-T1-O2d		104.4(1)	104.3(1)	104.3(1)	104.2(1)	104.4(1)	104.6(1)
O2-T1-O3		110.9(1)	111.2(1)	111.2(1)	111.2(1)	110.7(1)	110.9(1)
O2d-T1-O3		111.0(1)	111.6(1)	112.1(1)	111.5(1)	111.7(1)	112.1(1)
⟨O-T1-O⟩		109.4	109.4	109.5	109.4	109.4	109.4
T2-O3	×4	1.675(2)	1.670(2)	1.656(2)	1.654(3)	1.638(3)	1.636(3)
O3-O3a	×2	2.617(3)	2.612(3)	2.595(3)	2.585(5)	2.537(4)	2.536(7)
O3-O3e	×2	2.739(4)	2.728(5)	2.708(5)	2.706(7)	2.689(6)	2.689(6)
O3-O3f	×2	2.844(3)	2.835(3)	2.808(3)	2.809(5)	2.794(4)	2.786(4)
⟨O-O⟩T2		2.733	2.725	2.704	2.700	2.673	2.670
O3-T2-O3a	×2	102.8(1)	102.9(1)	103.1(1)	102.7(1)	101.5(1)	101.6(1)
O3-T2-O3e	×2	109.7(1)	109.6(1)	109.6(1)	109.8(2)	110.3(2)	110.5(2)
O3-T2-O3f	×2	116.2(1)	116.2(1)	115.9(1)	116.2(1)	117.0(1)	116.7(1)
⟨O-T2-O⟩		109.6	109.6	109.5	109.6	109.6	109.6
A-A		0.174(3)	0.248(5)	0.353(4)	0.304(6)	0.393(2)	0.51(2)
A-B		2.82(3)	2.85(2)	2.92(2)	2.88(3)	2.56(2)	2.75(2)
B-B		1.12(5)	0.96(4)	0.69(4)	0.82(5)	1.38(4)	1.39(4)
T1-T2		2.956(1)	2.947(1)	2.933(1)	2.937(1)	2.914(1)	2.912(1)

Note: a = x, $1 - y + x$, $½ - z$; b = $y - x$, y, $½ - z$; c = $1 - y$, $1 - y + x$, z; d = $x - y$, x, z; e = $-x$, $1 - y$, z; f = $-x$, $y - x$, $½ - z$.

only one type of ring in any one member of this family of nets (in more complex nets, this condition is relaxed). The symmetry, topological and geometrical properties of these nets are given in Table 6.

The first point of interest is the occurrence or nonoccurrence of these possible structure types. Two of these nets represent known structures: net 279 is the milarite structure type, and net 291 is the framework of steacyite, $(K,□)Th[(Na,Ca)_2Si_8O_{20}]$ (Richard and Perrault, 1972; Perrault and Szymanski, 1982). There are as yet no known minerals based on the other nets. Also indicated in Table 6 is net 278, the basis for the beryllo-silicate framework of beryl. Figure 3 shows the tetrahedral frameworks of beryl and milarite, together with their corresponding nets and the sigma-transformation that generates net 279 from net 278. The range of chemical compositions found for the milarite-type framework is very wide (see Table 7),

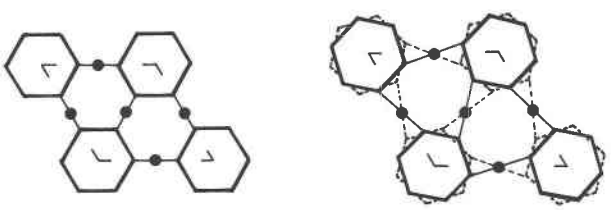

Fig. 1. Net 278: (**a**) projection down the **c** axis; successive lattice-translationally equivalent plane nets are stacked along the **c** axis and are linked by the two-connected vertices inserted into the prototype plane nets; in this net, the T2 polyhedron is square-planar; (**b**) projection down the **c** axis; alternate plane nets along the **c** axis are contrarotated 30° in opposite directions such that the T2 polyhedron is tetrahedral. Note that the difference between **a** and **b** is geometrical but not topological, and so the essential topological information is contained in **a**.

TABLE 6. Simple four-connected three-dimensional nets containing double rings of tetrahedral vertices

Net	Circuit symbol	Z	Space group	a (Å)	c (Å)	D	Ring size
278	$(46^5)_2(4^26^28^2)_1$	18	*P6/mcc*	10	9	40.4	6
279	$(4^26^4)_4(6^49^2)_1$	30	*P6/mcc*	10	14	40.4	6
287	$(34^26^3)_4(6^410^2)_1$	30	*P6/mcc*	13	14	68.3	3
289	$(4^26^4)_4(6^6)_1$	40	*P4/mcc*	11	14	42.4	8
291	$(4^36^3)_4(6^410^2)_1$	20	*P4/mcc*	8	14	44.8	4
297	$(4^26^4)_4(6^6)_1$	60	*P6/mcc*	16	14	51.7	12
299	$(4^26^4)_4(6^6)_1$	60	*P6/mcc*	16	14	51.7	6
301	$(4^36^3)_4(6^49^2)_1$	60	*P6/mcc*	16	14	51.7	4

Note: Net = net number assigned by Hawthorne and Smith (1986); Z = number of four-connected vertices in unit cell; D = volume per tetrahedral vertex.

yet the minerals all prefer this framework over the remaining frameworks. What factors are instrumental in the apparent stability of the milarite framework as compared with the other frameworks of Figure 2? One could, in principle, calculate the total energies of the frameworks, find some basis to normalize these for comparison, and see if the milarite framework has the lowest energy. However, this gives no insight into the structural reason(s) why one framework is to be preferred over another. It is of more use to see if the topological characteristics of the nets give any clues as to this relative stability. Inspection of Figure 2 shows one very obvious feature that varies significantly from structure to structure: some of the structures are much more open than others. As a measure of this, the volume per vertex for each net is given in Table 6. Three of the nets (279, 289, and 291) have significantly higher vertex densities (lower volume per vertex), and two of these three nets (279 and 291) are represented by natural minerals (Table 7). Structures that are very open (i.e., have large rings of tetrahedra) must have some feature that prevents them from collapsing in on themselves. Net 279 (milarite) has six-membered silicate rings and nine-membered silicate-beryllate rings, each of which is arranged coaxially along [001] to form a hollow tube. As indicated in Figure 3, these tubes contain the A, B, C, and D sites; these are occupied by alkali and alkaline earth cations and by H_2O groups, which thus support the fairly open framework. Net 291 (steacyite) has four-membered silicate rings and 12-membered silicate-sodiate rings that are stacked coaxially along [001] to form hollow tubes. The four-membered rings seem small enough not to need internal buttressing, and the 12-membered rings contain K and Th, both quite large cations. The other lower volume net is 289, which has eight-membered (silicate-type) rings and both six- and 12-membered mixed rings; the similarity of this to the steacyite structure suggests that this is a potential structure type of similar (but probably more complex) composition.

The other nets are very different; their types of rings

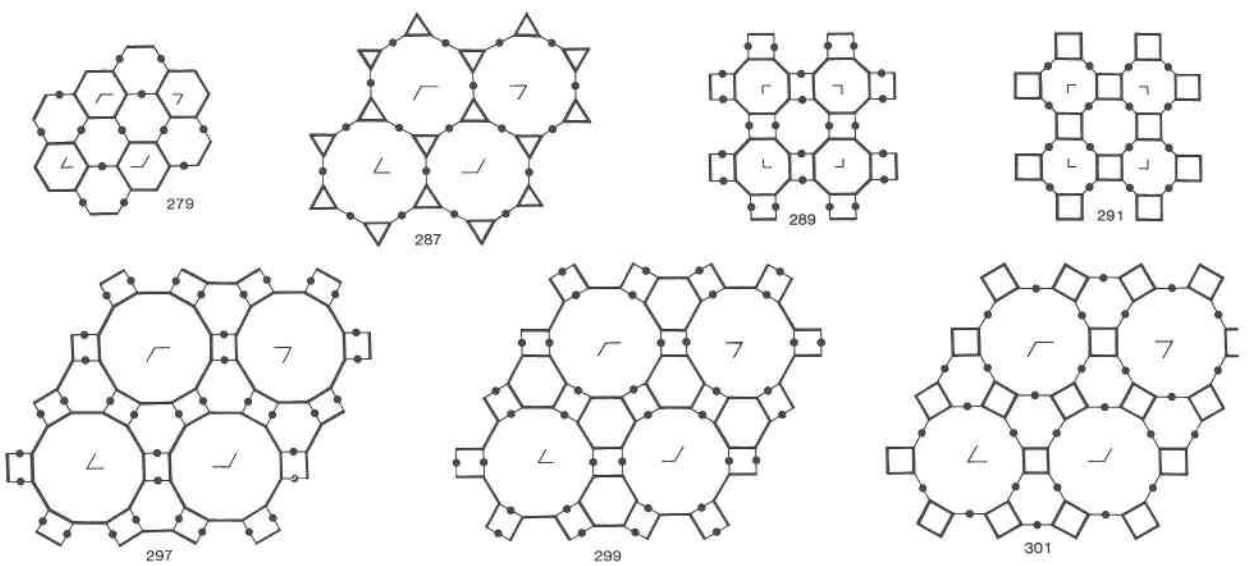

Fig. 2. Simple four-connected three-dimensional nets with double *n*-membered rings derived by systematic insertion of two-connected vertices into three-connected two-dimensional nets followed by sigma-transformations; nets are from Hawthorne and Smith (1986).

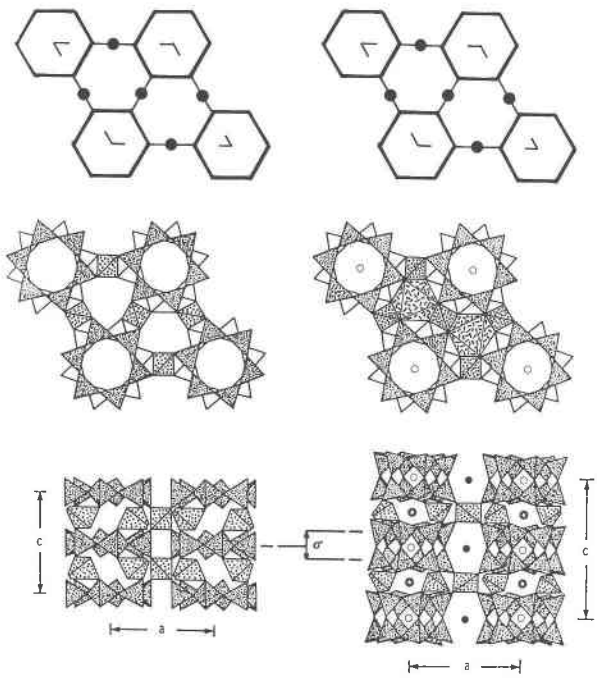

Fig. 3. Nets 278 and 279 and their relationship to the structures of beryl and milarite, together with the character of the sigma-transformation.

are summarized in Table 6. It is notable that most have large rings (up to 18-membered mixed rings) that stack along [001] to form very large open tubes. Open tubes of this sort are not known in natural minerals. Such large tubes can occur (e.g., cacoxenite, Moore and Shen, 1983), but they are filled with (ordered or disordered) cations or complex oxyanions that hold the tubes open. This suggests that structures based on these nets could occur if the open tubes were filled, possibly with large oxyanions or H-bonded complexes of H_2O groups (e.g., Bissert and Liebau, 1987).

TABLE 8. Site occupancies in the milarite-group minerals

Site	Equi-point	C.N.	Occupancy
T1	24m	4	Si, Al
T2	6f	4	Li, Be, B, Mg, Al, Si, Mn^{2+}, Zn
A	4c	6	Al, Fe^{3+}, Sn^{4+}, Mg, Zr, Fe^{2+}, Ca, Na, Y, REE
B	4d	9	Na, H_2O, □, Ca?, K?
C	2a	12	K, Na, Ba, □, Ca?
D	2b	18	□, ?

The cation occupancies of the two types of tetrahedral vertex for the minerals of the milarite group are shown in Table 8. It is immediately apparent that Si orders at the three-connected vertices of the prototype nets, whereas the other tetrahedrally coordinated cations order (almost exclusively) at the two-coordinated vertices of the prototype net. The unusual characteristic of this particular structure type is the wide variety of tetrahedrally coordinated cations incorporated into the structure.

H_2O IN MILARITE

Typical spectra for milarite in the midinfrared region are shown in Figures 4 and 5; the spectra are similar for all milarite samples, but with different absolute intensities of the absorption bands and, with minor shifts in band position. The bending mode at 1624 cm^{-1} and the combination mode at 5180 cm^{-1} can arise only from H_2O groups, and the stretching modes around 3550 cm^{-1} can also be assigned to H_2O. Thus the H in the milarite structure occurs as H_2O and not OH. The band at 5180 cm^{-1} results from a combination of the fundamental bending (ν_2) and asymmetric stretching (ν_3) modes, and it is polarized in the H-H direction of the H_2O group (assuming

TABLE 7. Minerals based on the nets of Table 6

Name	Formula	a (Å)	c (Å)	Space group	Net no.*	Reference
Armenite	$BaCa_2[Al_6Si_9O_{30}]2H_2O$	10.69	13.90	*P6/mcc*	279	(1)
Brannockite	$KSn_2[Li_3Si_{12}O_{30}]$	10.002(2)	14.263(3)	*P6/mcc*	279	(2)
Chayesite	$K(Mg,Fe^{2+})_2[(Mg,Fe^{2+})_2Fe^{3+}Si_{12}O_{30}]$	10.153(4)	14.388(6)	*P6/mcc*	279	(3)
Darapiosite	$KNa_2Zr[Li(Mn,Zn)_2Si_{12}O_{30}]$	10.32	14.39	*P6/mcc*	279	(4)
Eifelite	$KNa_3Mg[Mg_3Si_{12}O_{30}]$	10.137(5)	14.223(6)	*P6/mcc*	279	(5)
Merrihueite	$(K,Na)(Fe,Mg)_2[(Fe,Mg)_3Si_{12}O_{30}]$	10.16(6)	14.32(6)	*P6/mcc*	279	(6)
Synthetic	$K_2Mg_2[Mg_2Si_{12}O_{30}]$	10.222(2)	14.152(2)	*P6/mcc*	279	(7)
Milarite	$KCa_2[AlBe_2Si_{12}O_{30}]H_2O$	10.396(1)	14.781(4)	*P6/mcc*	279	(8)
Osumilite	$(K,Na)(Fe,Mg)_2[(Al,Fe)_3(Si,Al)_{12}O_{30}]$	10.150(2)	14.289(2)	*P6/mcc*	279	(9)
Osumilite-(Mg)	$(K,Na)(Mg,Fe)_2[(Al,Fe)_3(Si,Al)_{12}O_{30}]$	10.078(2)	14.319(2)	*P6/mcc*	279	(9)
Poudretteite	$KNa_2[B_3Si_{12}O_{30}]$	10.253(1)	13.503(4)	*P6/mcc*	279	(10)
Roedderite	$(Na,K)(Mg,Fe)_2[(Mg,Fe)_3Si_{12}O_{30}]$	10.142(5)	14.319(3)	*P62c*	279	(11)
Sogdianite	$(K,Na)_2(Zr,Fe,Ti)[Li_2(Li,Al)Si_{12}O_{30}]$	10.083(5)	14.24(1)	*P6/mcc*	279	(1)
Sugilite	$(K,Na)(Fe^{3+},Al)_2[Li_3Si_{12}O_{30}]$	10.009(2)	14.006(3)	*P6/mcc*	279	(2)
Yagiite	$(Na,K)Mg_2[(Al,Mg)_3(Si,Al)_{12}O_{30}]$	10.09(1)	14.20(3)	*P6/mcc*	279	(12)
Steacyite	$(K,□)Th[(Na,Ca)_2Si_8O_{20}]$	7.58(1)	14.77(2)	*P4/mcc*	291	(13, 14)

Note: References: (1) Bakakin et al. (1975); (2) Armbruster and Oberhänsli (1988b); (3) Velde et al. (1989); (4) Semenov et al. (1975); (5) Abraham et al. (1983); (6) Dodd et al. (1965); (7) Khan et al. (1971); (8) this study; (9) Armbruster and Oberhänsli (1988a); (10) Grice et al. (1987); (11) Armbruster (1989); (12) Bunch and Fuchs (1969); (13) Richard and Perrault (1972); (14) Perrault and Szymanski (1982).

* The net number is from Hawthorne and Smith (1986).

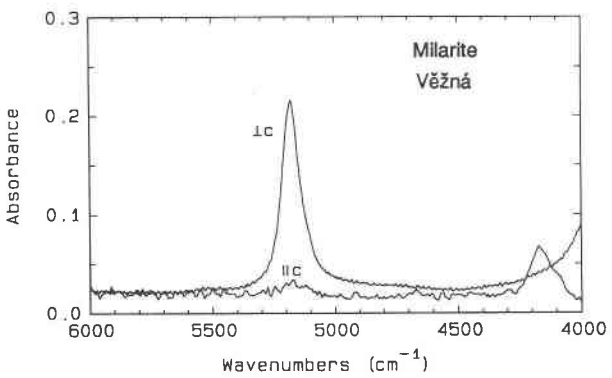

Fig. 4. Infrared spectra of milarite from Věžná in the near-infrared region for a crystal thickness of 150 μm.

C_{2v} symmetry). The polarization of this band in a direction perpendicular to the **c** axis shows that the H-H vector of the H_2O group is aligned perpendicular to **c**. Likewise, the asymmetric stretch (ν_3) at 3581 cm^{-1} is polarized perpendicular to the **c** axis (Fig. 5a), confirming the H-H orientation as perpendicular to **c**. Next we must identify the orientation of the plane containing the three component atoms of the H_2O group. This may be done from the fundamental modes, as the bending mode (ν_2) and the symmetric stretch (ν_1) are polarized along the (ideal) twofold axis of the H_2O group; identification of this direction, in combination with the already known direction of the H-H vector, fixes the orientation of the H_2O group. The bending mode is polarized parallel to **c** (Fig. 5b), indicating that the twofold axis of the H_2O group is parallel to **c**; this fixes the H_2O plane as parallel to the **c** axis. This corresponds to the type II (H_2O) found in beryl (Wood and Nassau, 1967) and cordierite (Goldman et al., 1977).

The one anomalous aspect of this assignment is the band at 3520 cm^{-1} assigned to ν_1. Unlike the analogous bands in the spectra of beryl and cordierite, which were highly polarized, this band in the milarite spectra shows little polarization dependence when the contribution of the 3580-cm^{-1} band is removed either by numerical curve fitting or by visual estimation. The incomplete polarization of the 1620-cm^{-1} band suggests that the diad axis of the H_2O group is not perfectly aligned with the **c** axis in milarite. In other minerals such as joaquinite (Rossman, 1975), in which an H_2O group was proposed on the basis of the infrared spectra, the polarizations of the individual H_2O bands were distinct. Likewise in cordierite (Goldman et al., 1977), the type II H_2O that most resembles the H_2O in milarite has distinct polarizations in its infrared spectra. It is difficult to assign the band at 3580 cm^{-1} convincingly to another H_2O species. If we try to do this,

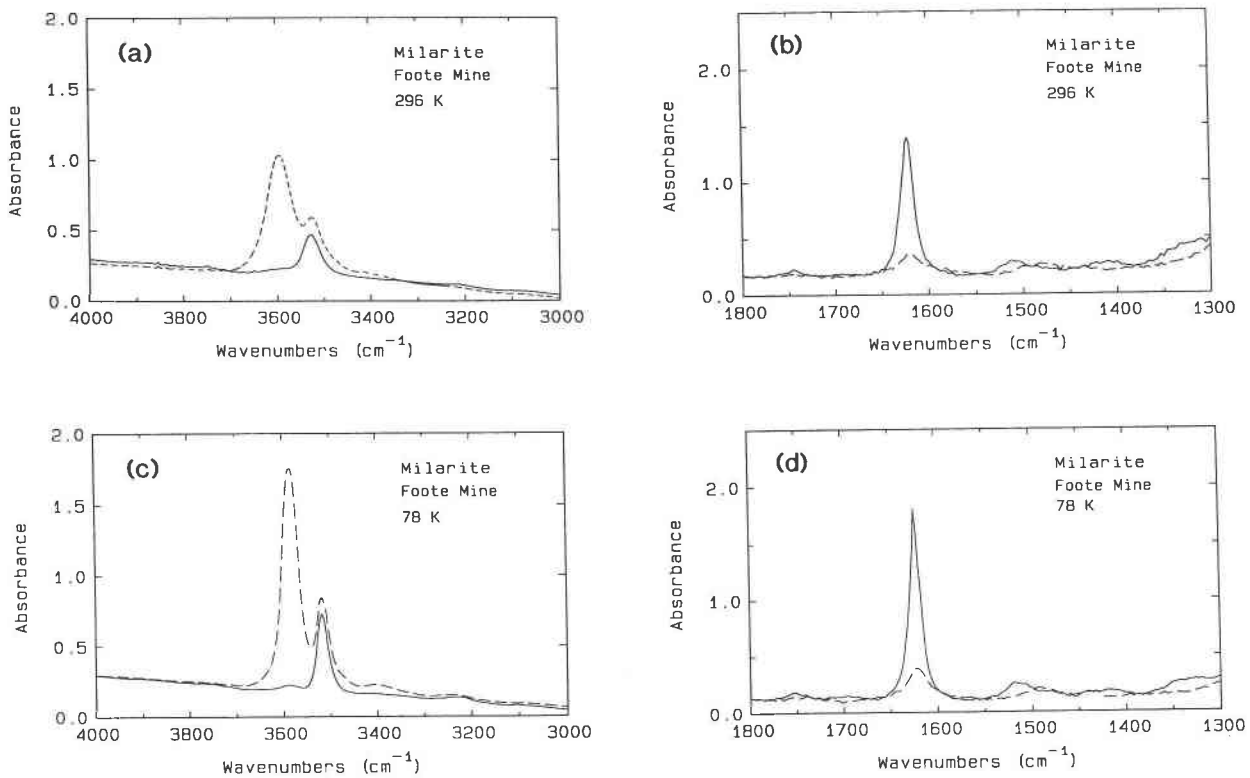

Fig. 5. Typical infrared spectra of milarite: (**a**) in the H_2O principal stretching region, solid line ∥**c**, dotted line ⊥**c**, sample 24 μm thick, 296 K; (**b**) in the H_2O symmetric bending region, solid line ∥**c**, dotted line ⊥**c**, sample 24 μm thick, 296 K; (**c**) as **a** at 78 K; (**d**) as **b** at 78 K.

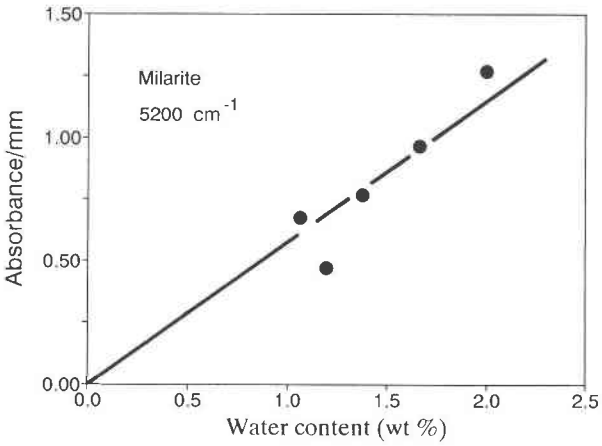

Fig. 6. The correlation between the intensity of the 5200 cm^{-1} band (polarized $\perp$**c**) and the H_2O content of milarites.

the lack of an asymmetric stretch in the **E**$\|$**c** spectrum would force the H-H direction to be $\|$**c**; the observed **E**$\|$**c** spectrum has no significant absorptions at ~5200 and ~1620 cm^{-1}, and hence is not compatible with such an orientation.

Two samples (Foote and Rössing) were made thin enough so that the spectra of the fundamental bands (ν_1, ν_2, and ν_3) could be recorded on scale. With these samples, it was possible to test whether the polarization behavior of the 3520-cm^{-1} band could be due to an unrecognized contribution from an OH component that, by coincidence, was superimposed on the 3520-cm^{-1} H_2O band. Although minor OH components are common in silicate minerals, their absolute intensity varies greatly among samples from different localities (e.g., olivine, Miller et al., 1987; pyroxene, Skogby et al., 1990). Thus it is to be expected that the ratios of the intensities of an H_2O band to those of a hypothetical OH band would vary from locality to locality. This is not the case with milarite. The intensity ratios of the ν_1 band and the two polarizations of the ν_3 band were identical within error of measurement, indicating that it is unlikely that an OH component is the cause of the unusual polarization behavior of the ν_3 band. The spectra of these two samples were recorded at 78 K. The peak height of the ν_1 and ν_3 bands (Figs. 5c and 5d) nearly doubled; this was not just due to narrowing of the bands because the integrated area also increased by about 25% in both polarizations. The peak height and integrated area of the ν_2 band increased by about 33%. Thus these polarization and intensity anomalies remain unexplained.

Using the H_2O contents given by Černý et al. (1980), there is a correlation between the intensity of the 5200-cm^{-1} band (**E** perpendicular to **c**) and the (H_2O) content (Fig. 6). In milarite from Rössing, Namibia, inclusions of other hydrous minerals are common, and hence it is not surprising that data for it deviate from the trend line to the side of higher analytical (H_2O) content. Similarly, many inclusions were observed in the Guanajuato milarite. From the trend line shown in Figure 6, the ϵ value from Beer's law is 4.2, a value significantly higher than that for (liquid) H_2O. Goldman et al. (1977) have previously noted that the intensity of this combination mode is inversely related to the strength of the H bonding for which the H_2O group is the donor anion. The effect of this is to enhance the sensitivity of the spectroscopic method to weakly bonded H_2O compared with H_2O in fluid inclusions.

Table 9. Absorption band positions and values for H_2O in milarite samples

Mode	Band position nm	Band position cm^{-1}	Polarization	ϵ values Val Giuf	Rössing	Foote
ν_1		3516	$\|$**c**, $\perp$**c**	—	93	55
ν_2		1624	$\|$**c**	—	240	211
ν_3		3581	$\perp$**c**	—	240	172
$\nu_2 + \nu_3$	1922	5203	$\perp$**c**	4.3	—	—
$(\nu_1 + \nu_2)$?	1948	5133	$\perp$**c**	sh*	sh*	sh*
Overtone	1477	6770	$\perp$**c**	0.05	—	—
Overtone	1438	6954	$\|$**c**, $\perp$**c**	0.11	—	—
Overtone	1403	7128	$\|$**c**	0.08	—	—

* Weak overlapping shoulder on the 1922-nm band.

The intensities of the midinfrared fundamental absorptions of the H_2O group were determined for the Rössing and Foote samples. Using the H_2O content obtained from the trend line in Figure 6, molar absorptivity (ϵ) values were calculated and are given in Table 9; they are similar in magnitude to those found for H_2O in cordierite (Goldman et al., 1977).

Chemical relations for milarite

Palache (1931) gave the ideal formula of milarite as $(K,Na)Ca_2Be_2AlSi_{12}O_{30}\cdot xH_2O$, $x = 0.75$. Černý et al. (1980) showed that Be is a variable component through the substitution $^{B}Na + {}^{T2}Be \rightleftharpoons {}^{B}\square + {}^{T2}Al$. However, Černý et al. (1991) show REE cations to be a significant substituent into the milarite structure through the substitution $^{A}(Y,REE) + {}^{T2}Be \rightleftharpoons {}^{A}Ca + {}^{T2}Al$. Thus the large cation substitutions can be quite complicated, and the tetrahedral framework can have significant variation in Be/(Be + Al) ratio. Nevertheless, the total tetrahedral cations must be 15 apfu in this structure type if vacancies are to be avoided at the tetrahedrally coordinated cation sites.

Framework-cation sums

It is apparent from the analyses of Table 1 that, based on a formula unit of 30 anions, the sum of the fourfold-coordinated species is not constant but varies in the range 14.85–15.26 apfu. There are two possibilities here: (1) data for one or more components in the chemical analyses are in error; (2) a significant component has not been considered in the analytical procedures. As the analyses span both sides of ideality, the omission of any important component cannot be the problem because this would shift all the sums either up or down and would not result in a wide spread around the ideal value, as is the case for

data for milarite. This leaves us with the possibility of error in one or more components, an error that is common to many analyses. As some of the milarite samples were analyzed both previously and as part of this work, we can get some indication of errors that could cause this deviation from the ideal sum of 15 apfu. The milarite sample furthest from ideality is sample 33, and both previous and current analyses indicate a fourfold-coordinated cation sum of 15.26 apfu. As the analyses were done by different methods in different labs, this indicates that the source of the error is unlikely to lie in the components analyzed in both studies. This essentially points to BeO as the culprit. Values of Be (and BeO) contents were calculated such that the sum of the framework cations is 15.00 apfu for a 30-anion renormalization procedure, excluding H_2O; these values are given as BeO_c in Table 1. We note that this problem is not restricted to this study but is also found in the data of Černý et al. (1980), which were measured in several different labs and also taken from the literature. The variation in framework cation sums is 14.71–15.25 apfu, reasonably similar to that observed in the present work.

An obvious correlation is apparent in the data of Černý et al. (1980). Figure 7 shows that the Si content (in atoms per formula unit) is apparently related to the Be/(Be + Al) ratio, as a very well developed correlation is observed. A similar correlation is apparent in the data of Table 1 for both Be and Be_c values. We consider the possibility of Be ⇌ Si substitution in the hexagonal rings as unlikely; when Be substitutes for Si in a structure, it invariably totally replaces Si at one structural position (often causing a change in space group) with no significant Be-Si solid solution at any one site. Alternatively, Al is known to substitute for Si in other minerals of this structure type, and the data do suggest small amounts of Al substitution for Si with variable Be content.

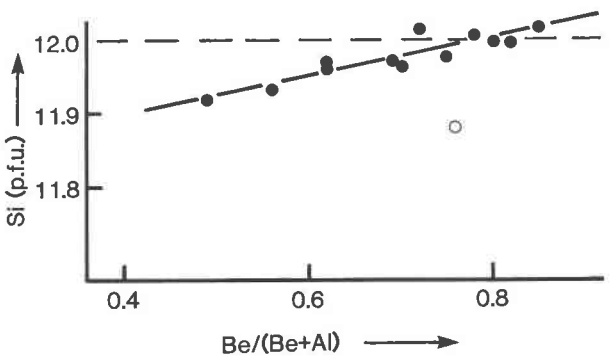

Fig. 7. Variation in Si (apfu) as a function of Be/(Be + Al) in milarites; the chemical data are taken from Černý et al. (1980). The open circle is the analysis of Tittling milarite (no. 33 of Černý et al., 1980); the analysis of this milarite sample given in Table 1 shows that this sample does lie on the observed trend.

Crystal chemistry of milarite

It is desirable to know the steric response of the structure to variations in mineral chemistry, as this is very useful for indicating chemical complications in a mineral (for example, the unusual chemical nature of the Y-rich milarite from Jaguaraçú, Brazil, was first recognized from its unusual stereochemistry) and also for understanding the structural controls on chemical substitutions in the mineral. Consequently we will examine in detail the stereochemistry of the cation sites in milarite.

The T1 tetrahedron

This is the tetrahedron of the $[Si_{12}O_{30}]$ double six-membered ring (Fig. 3). It shares three corners with adjacent T1 tetrahedra and one corner with a T2 tetrahedron that links the $[Si_{12}O_{30}]$ clusters into a framework. For the milarites refined here and in the refinements of Černý et al. (1980), the grand ⟨T1-O⟩ distance is 1.611 Å with a total spread of ±0.002 Å. This indicates that, in all of the milarites examined here, there is no significant variation in the site occupancy of the T1 position. The chemical analyses of all these milarites have a grand mean Si content of 11.93 apfu. The chemical analyses of Černý et al. (1980) suggest a more complicated situation. Figure 7 shows the variation in Si apfu as a function of Be/(Be + Al); there is a well-developed positive correlation between these parameters, indicating that the Si content of milarites is not fixed at 12 atoms pfu but is a function of the Be/(Be + Al) ratio. It may be significant that the Be/(Be + Al) ratio of normal milarites does not greatly exceed 0.8, the point at which the observed trend intersects the maximum possible value of 12 Si apfu. Only the Si value for the Tittling milarite sample (no. 33 of Černý et al., 1980) does not plot on the trend, and the reanalysis of this material given in Table 1 shows that it does in fact plot on the observed trend. One particular milarite sample does not plot on the trend of Figure 7; no. 13 of Černý et al. (1980), originally reported by Iovcheva et al. (1966), has only 10.76 Si apfu and an extremely large amount of Al (2.60 apfu), suggesting extensive substitution of Al for Si at the T1 site. However, as this particular analysis is the only one of its type, further examination of this material is desirable.

How does the trend of Figure 7 agree with our conclusions relating to the ⟨T1-O⟩ distances in milarites? The maximum Al substitution in the analyses of Figure 7 is 0.16 Al apfu; this amount of Al would produce an increase in mean bond length of ~0.0017 Å, a very tiny amount that is within the spread of ±0.002 Å observed for all the refined milarite structures. Thus, although the chemical analyses do suggest a very small amount of Al ⇌ Si substitution at the T1 site in milarites, it is not enough to affect significantly the size of the T1 tetrahedron.

The T2 tetrahedron

This is the tetrahedron that links the $[Si_{12}O_{30}]$ clusters into a framework (Fig. 3); it shares four corners with ad-

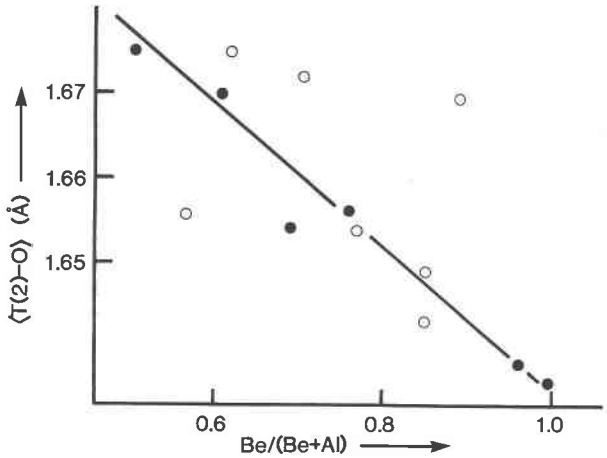

Fig. 8. Variation in ⟨T2-O⟩ as a function of Be/(Be + Al) in milarites; filled symbols indicate site occupancies derived from unconstrained site-occupancy refinement, and hollow symbols denote occupancies derived from the chemical analyses.

jacent T1 tetrahedra and two edges with adjacent A octahedra. Previous refinements have shown that this site is occupied by variable amounts of Be and Al, and the scattering observed at this site in the present study is consonant with this assignment.

The T2 site occupancies can be determined in two ways: (1) Unconstrained site-occupancy refinement can be used to determine the occupancy in terms of Be and Al. (2) Based on data from the chemical analyses, all Be can be assigned to T2 and the remainder of the site filled with Al; when Be + Al = 3, the contents must be normalized to 3.0 apfu.

Figure 8 shows the ⟨T2-O⟩ distance as a function of the Be/(Be + Al) ratio for the structures refined in this study, using the results of the unconstrained site refinements to determine the Be/(Be + Al) ratio (solid circles); the ideal relationship for a hard-sphere model is also shown. Thus the size of the T2 tetrahedron is linearly related to the Be-Al contents. If ⟨T2-O⟩ is plotted against the chemically analyzed values of the Be-Al content (Fig. 8, hollow circles; previous literature data are also shown in this manner), there is far more scatter, although the values do lie about the relationship defined by the refined site compositions and the hard-sphere model in Figure 8. There are two possibilities here; either the milarite samples are usually quite heterogeneous and the crystals used for the structure work where in general not representative, or the Be analyses leave something to be desired. Whichever is the case, it is apparent that the T2 tetrahedral size responds to variations in Be-Al occupancy.

The A octahedron

The A octahedron lies between the $[Si_{12}O_{30}]$ clusters, sharing corners with the T1 tetrahedra and further strengthening the framework linkage. It also shares edges

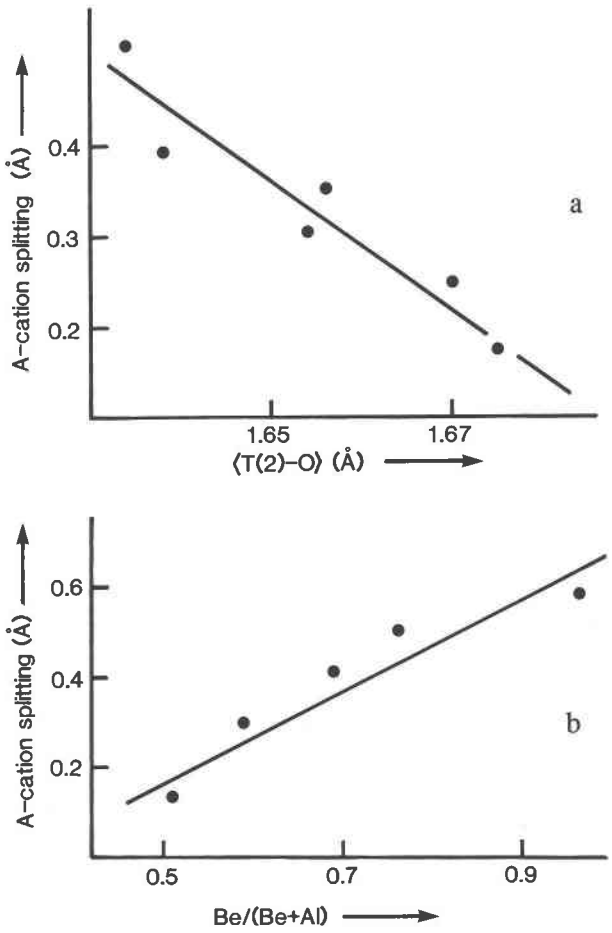

Fig. 9. The variation in A-cation splitting in milarites: (**a**) as a function of the ⟨T2-O⟩ distance; (**b**) as a function of Be/(Be + Al).

with three flanking T2 tetrahedra (Fig. 3), edges that are extremely contracted relative to the other edges of both the A octahedron and the T2 tetrahedron. In normal milarite, this site is ideally completely occupied by Ca; both chemical analyses and the unconstrained site-occupancy refinements confirm this. In all the refinements described here, the A cation showed extremely anisotropic displacement parameters with the long axis of the ellipsoid oriented along the **c** axis; similar behavior was noted by Černý et al. (1980). In the present work, this was modeled by a split atom (cf. Kimata and Hawthorne, 1989; Armbruster et al., 1989). The amount of splitting varies across the series (Fig. 9), using either ⟨T2-O⟩ or Be/(Be + Al) as a measure of the Be content. In milarites 36 and 37, the A site is partly occupied by Y and REE. Nevertheless, the constituent cation(s) still shows the splitting, and the amount of splitting still increases as a function of the Be/(Be + Al) ratio.

In normal milarites, with a split-site model and variable anisotropic displacement parameters, unconstrained site-occupancy refinement converged to complete occu-

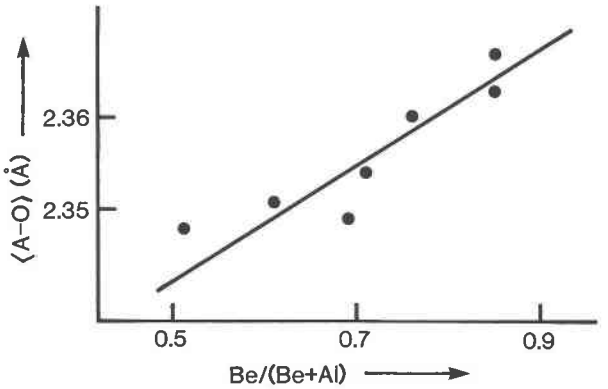

Fig. 10. The variation in ⟨A-O⟩ as a function of Be/(Be + Al) in milarites.

TABLE 10. Comparison of refined and chemically assigned B-site occupancies for the milarite samples refined here

Species	25	33	35	30
Na*	0.46(4)	0.64(4)	1.10(4)	0.89(6)
Na	0.06	0.18	0.46	0.13
H_2O	0.67	0.72	0.92	0.94
Ca	0.04	—	—	0.11
K	0.05	0.06	—	—
(Na + H_2O)**	0.46	0.61	1.01	0.69
(Sum)†	0.61	0.71	1.01	0.88

* Indicates refined occupancy.
** Effective scattering power of chemically analyzed (Na + H_2O) (expressed as Na at sin $\theta/\lambda = 0.30$).
† Effective scattering power of all scattering species assigned to B from the chemical analysis.

pancy of the A site by Ca. For the yttrium-REE milarite samples, the A-site occupancy converged to values consonant with the microprobe analyses of the crystals used for the X-ray intensity data collection. For normal milarites, the grand ⟨A-O⟩ distance is 2.366 Å with a total spread of ±0.010 Å, but there is a pronounced correlation (Fig. 10) with the Be/(Be + Al) ratio of the milarite, a significant inductive effect. The ⟨A-O⟩ distances for the yttrium-REE milarites are significantly less than the ⟨A-O⟩ distances in normal milarites, the effect of substituting Y^{3+} (r = 0.90 Å) for Ca (r = 1.00 Å) (Shannon, 1976).

Armbruster et al. (1989) have studied the reason for the A- and B-site splitting in milarite by refining the structures of both natural and dehydrated milarite. In dehydrated milarite, both the A- and B-site splittings do not occur. This can be rationalized as follows (Armbruster et al., 1989). If H_2O occupies the split B site and the B cations occupy the central B site, dehydration will remove the H_2O from the split site but will not affect the B cations at the central B site. This is what is observed in dehydrated milarite, leading to the conclusion that H_2O occupies the split B site. On dehydration, the splitting of the A site also does not occur. This suggests that the A-site splitting observed in milarite is the result of a ^{A}Ca-$^{B}H_2O$ interaction along the $\bar{6}$ axis, and Armbruster et al. (1989) propose that the A site (= Ca) is coordinated by seven anions, with a Ca-H_2O bond of 2.84 Å augmenting the six shorter (2.35 Å) Ca-O bonds, and that the lowering of symmetry that gives rise to the well-known optical anomalies in milarite is due to the polar nature of the A-site coordination and the resulting disorder along ±**c**. If this is the case, it is possible that there is a high-temperature ferroelastic phase transition in milarite. At high temperatures, the A cation is eightfold coordinated; at a specific temperature, there is the onset of disorder at the A and B sites that breaks the symmetry and gives rise to the polar nature of the A-cation coordination. This transition is suggested by the fact that the directional disorder of the Ca-H_2O bond is not sufficient to break the hexagonal symmetry, as such ordering is possible in noncentrosymmetric hexagonal subgroups of *P6/mmc*. Thus there must be additional factors (e.g., spontaneous strain) affecting the breaking of hexagonal symmetry.

The B polyhedron

The B site lies on the threefold axis, between the $[Si_{12}O_{30}]$ clusters, and directly above and below the A octahedron (Fig. 3), surrounded by nine O atoms. The ideal B site occurs at $z = 0$, and it has three O neighbors at ~2.78 Å and six O neighbors at ~3.30 Å. In the refinements described here (and in the refinements by Bakakin et al., 1975, and Černý et al., 1980), the B cations showed very anisotropic displacement behavior that was modeled by a split-atom position; note that for the B cation, the splitting is much greater than that observed for the A atoms.

Bakakin et al. (1975) and Černý et al. (1980) have shown that H_2O is an important constituent at the B site. However, small amounts of alkali and alkaline earth cations are also assumed to occupy this site. Indeed, Černý et al. (1980) show that the incorporation of cations in the ideally empty B polyhedron is the only charge-compensation mechanism for the incorporation of Be at T2 in excess of the ideal amount of 2 apfu. Note that this does ignore substitutions of the type $(Y,REE)^{A} + Be^{T2} \rightleftharpoons Ca^{A} + Al^{T2}$; however, these are not of significance in normal milarites. Armbruster et al. (1989) have shown that the split B site is occupied by H_2O and that the B cations occupy the central B site. In the structure of the dehydrated milarite sample, they also showed that the B site does incorporate K. Table 10 compares the refined scattering power at the B site with the excess cations and H_2O assigned to the B site from the chemical analysis; by and large, there is reasonably good overall agreement between the two sets of data.

The C polyhedron

The C site occurs on the sixfold axis at $z = \frac{1}{4}$, sandwiched between two $[Si_{12}O_{30}]$ clusters (Fig. 3); the central atom is bonded to 12 O atoms, all of which are at a distance of ~3.0 Å. This site is occupied completely by K, as indicated by both chemical analyses and uncon-

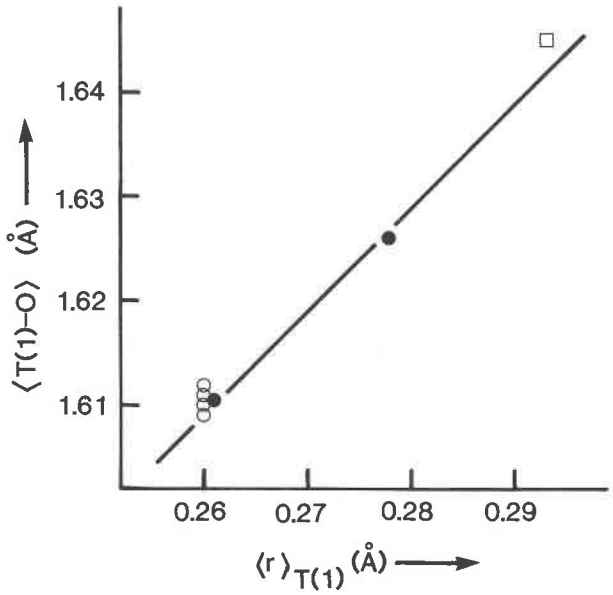

Fig. 11. Variation in ⟨T1-O⟩ with constituent cation radius at the T1 site for the milarite-group minerals; the filled circles are the mean values of the data for milarites and osumilite, and the line is drawn through these two points; other data are marked by hollow symbols, except the open square = armenite.

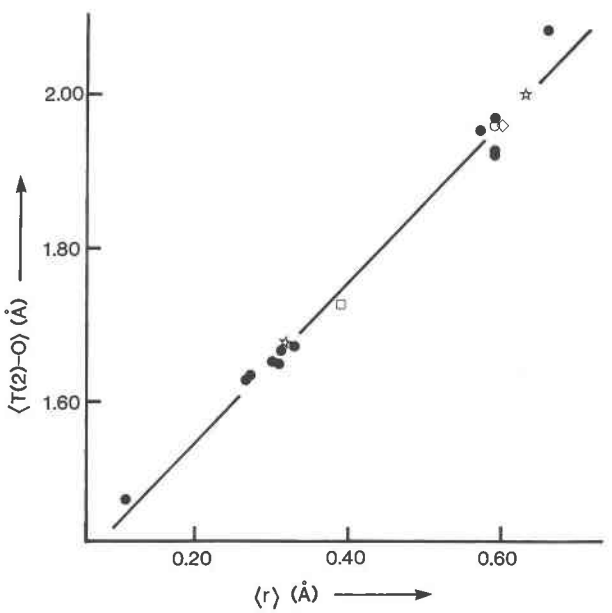

Fig. 12. Variation in ⟨T2-O⟩ as a function of constituent cation radius at the T2 site for the milarite-group minerals; filled circles are data points that we consider more reliable, and the stars indicate data for the related structures of lithium cesium beryl (Hawthorne and Černý, 1977) and tuhualite (Merlino, 1969); data for zektzerite (Ghose and Wan, 1978) also lies on the line; open circle = sogdianite, open square = armenite, open diamond = zinc milarite.

strained site-occupancy refinements. Unlike the A and B cations, the C cation is not significantly displaced from the high-symmetry position at the center of the C polyhedron.

The D polyhedron

The D site occurs at the center of the $[Si_{12}O_{30}]$ cluster (Fig. 3), surrounded by 18 O atoms arranged at the vertices of an augmented hexagonal prism. In this study, no significant density was detected within this cavity, although if small amounts of atoms were disordered about this cavity, it would be extremely difficult to detect them with conventional diffraction techniques.

Stereochemistry of the milarite structure type

As is apparent from Table 7, the group of double-ring silicates with symmetry *P6/mcc* and general formula $^{[6]}A_2{}^{[9]}B_2{}^{[12]}C^{[18]}D^{[4]}T2_3{}^{[4]}T1_{12}O_{30}(H_2O)_x$ is quite large. Much of the earlier mineralogical work on this group refers to the minerals of the milarite group, whereas some of the more recent work refers to minerals of the osumilite group. Frequency of usage inclines us to the former designation. In addition, milarite has more of the possible cation sites filled [A, B, C, T1, and T2] than does osumilite [A, C, T1, and T2], which makes milarite more useful as the type structure. Consequently we designate these minerals as belonging to the milarite group. The cation sites and the range of species that occupy them are summarized in Table 8.

The T1 tetrahedron

Most of the milarite-group minerals have the T1 site ideally occupied by Si. However, armenite, osumilite, and yagiite incorporate significant amounts of Al at T1, and the ⟨T1-O⟩ distance should reflect this substitution. Figure 11 shows the variation in ⟨T1-O⟩ as a function of Al assigned to T1 from the chemical analyses. There is a well-developed linear relationship between tetrahedral size and Al content. The line shown in the figure is not a least-squares line but was drawn through the average values for milarite (this study; Černý et al., 1980) and osumilite (Armbruster and Oberhänsli, 1988a; Hesse and Seifert, 1982). The slope of this line is 1.0, the ideal value for a hard-sphere model, and the relationship is given by $\langle T1\text{-}O\rangle = 1.609 + 1.0\ \langle r_{T1}\rangle$ where $\langle r_{T1}\rangle$ is the mean constituent ionic radius of the T1 cations. This may also be expressed as a predictive relationship for the amount of Al at the T1 site: $Al_{T1} = 7.7[\langle T1\text{-}O\rangle - 1.609]$. This equation could be refined somewhat by further structural work on well-characterized samples of armenite.

The T2 tetrahedron

The T2 site shows a tremendous range in occupancy (Table 8) both with regard to size ($B^{3+} \rightarrow Fe^{2+}$) and formal valence ($Li^{+} \rightarrow B^{3+}$). Figure 12 shows the ⟨T2-O⟩ distance as a function of the constituent cation radius; a linear

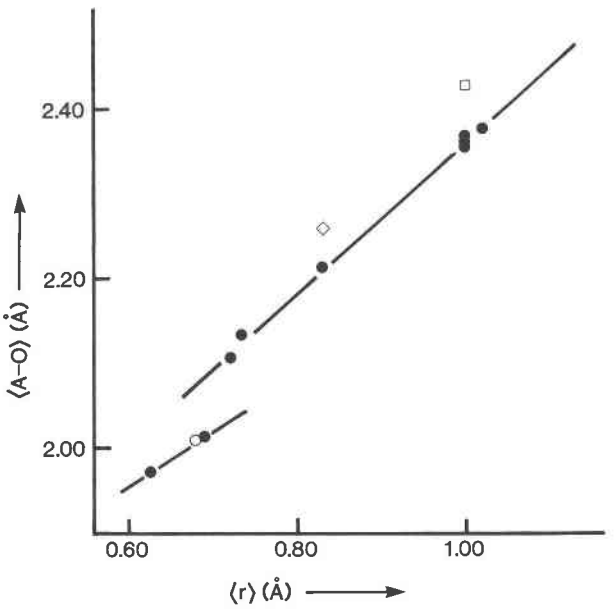

Fig. 13. Variation in ⟨A-O⟩ as a function of constituent cation radius at the A site for the milarite-group minerals; legend as for Figure 12. The data points seem to define two separate correlations.

correlation is apparent, and linear regression gives the relationship

$$\langle \text{T2-O} \rangle = 1.344 + 1.039 \langle r_{T2} \rangle \qquad R = 0.992.$$

Despite this apparently good result, there are significant discrepancies that suggest that the situation may be more complicated than it seems; there are significant deviations from linearity for several well-refined structures, and a more detailed discussion seems warranted.

The ⟨T2-O⟩ values for brannockite are ~0.05 Å less than those for sugilite and sogdianite when the T2 site in all these minerals is occupied solely by Li. Let us consider the data for these refinements. There are two precise refinements for brannockite (Armbruster and Oberhänsli, 1988b) giving similar results. In further support of this, Hawthorne (unpublished data) refined the brannockite structure some years ago, and these results are in good agreement with those of Armbruster and Oberhänsli (1988b). The observed bond lengths in brannockite would seem to be reliable. White et al. (1973) show that brannockite (from the Foote mine, the only known locality) is of ideal composition, indicating that the T2 site should be completely occupied by Li. This is also supported by the refinements, which give reasonable equivalent isotropic displacement parameters for T2 completely occupied by Li.

Next we consider sugilite. The structure of sugilite from the Wessels mine, South Africa, was refined by Armbruster and Oberhänsli (1988b), and that of sugilite from Iwagi Islet, Japan, was refined by Kato et al. (1976). The ⟨T2-O⟩ distances in both refinements are essentially the same, suggesting that the value given above is reliable. In the analysis of the Wessels material, Li was not analyzed but was assumed to fill the T2 site; the equivalent isotropic displacement parameter supports this assignment. The original analysis of the Iwagi Islet sugilite indicated significant Al and Fe^{3+} at the T2 site, but the observed ⟨T2-O⟩ distance was not compatible with this. Reanalysis of the material (T. Kato, personal communication, 1984) gave a significantly higher value for Li, but it was not sufficient to fill T2; however, the refinement indicated Li essentially completely occupying T2. Refinements of Iwagi sugilite and an Indian sugilite (T. Kato, personal communication, 1989) give values close to the relationship of Černý et al. (1980) and hence close to the values for the Wessels sugilite. Thus the values for sugilite also seem reliable. A reinvestigation of sogdianite is desirable.

To summarize the situation for brannockite and sugilite, the T2 site is occupied completely by Li in both structures, with ⟨T2-O⟩ distances of 1.922 and 1.971 Å, respectively. The principal difference between these two structures is that the B site is unoccupied in brannockite and completely occupied by Na in sugilite. Thus the presence of Na at B in sugilite could inductively affect the size of the T2 tetrahedron. Such inductive effects are much more pronounced for low-valence cations such as Li than for higher-valence cations such as those that occupy T2 in the other milarite-group minerals; presumably this is why such effects are less noticeable or possibly absent in the rest of the milarite-group structures.

Data for poudretteite deviate from a linear relationship in Figure 12 by ~0.02 Å and yet the structure is very well refined. In fact, the data below $\langle r \rangle = 0.35$ Å (poudretteite, milarite samples) define a very well developed linear trend with a slope of ~1.0, slightly less than the slope for the total data set. It is possible that the relationship is slightly nonlinear over the whole range.

The A octahedron

The A site also shows a wide range of cation occupancy (Table 8) with a concomitant range of polyhedral size. Figure 13 shows the ⟨A-O⟩ distance as a function of constituent cation radius; ignoring the imprecise values for armenite and zinc milarite, we can fit a linear model with a correlation coefficient of 0.983 and a form $\langle \text{A-O} \rangle = 1.311 + 1.066 \langle r_A \rangle$ where $\langle r_A \rangle$ is the mean radius of the constituent A cations. However, the deviations from linearity are considerable; for example, data for both brannockite and osumilite deviate from the line by ~0.04 Å, an amount far greater than the precision of the values. On the other hand, a good linear model occurs if the relationship is broken into two segments, as shown by the full lines in Figure 13. The reason for this is not clear.

The B polyhedron

In milarite itself, the B site plays a key role in the principal substitution in the structure $Na^B + Be^{T2} \rightleftharpoons \square^B + Al^{T2}$. In some of the other milarite-group minerals, the B site is empty (e.g., brannockite); in others (e.g., sugilite), it is full. When occupied by a cation, it is (always?) oc-

cupied by Na, which often shows a displacement from the center of the polyhedron along the c axis.

The C polyhedron

This polyhedron is occupied primarily by K (and possibly minor Na) in all the milarite-group minerals except armenite, in which it is occupied by Ba. The occurrence of Ba at the C site is related to the occurrence of significant amounts of Al at the T1 site; the higher valence cation at C helps satisfy the local bond-valence efficiency at the O2 anion caused by the substitution of the lower-valence Al at the T1 site.

Paragenesis of milarite

Milarite is found in a variety of environments, from vugs in plutonic rocks through diverse pegmatites to hydrothermal ore deposits and alpine veins. Before we can make any general observations, a brief review of specific localities is in order.

Principal milarite localities

Postorogenic to anorogenic intrusions of alkaline affinity, together with their interior pegmatites, constitute a distinct type of milarite-generating environment. Vugs in nordmarkite at Ramnes and in the Grorud and Tysfjord districts of Norway (R. Kristiansen, personal communication, 1989; Oftedal and Saebö, 1965; Raade, 1966) and miarolitic pegmatites in the Strzegom granite, Poland (Janeczek, 1986), the Kent granite in Central Kazakhstan (Chistyakova et al., 1964), the Conway granite, New Hampshire (J. S. White, personal communication, 1985), and the Strange Lake syenite, Labrador (Černý et al., 1991), all have milarite on a potassium feldspar–quartz substrate associated with albite, zeolites, fluorite, stilpnomelane, wulfenite, and rarely other Be minerals such as beryl, bazzite, helvite, bertrandite, phenacite, or bavenite. Milarite is also found in marble xenoliths in a nepheline-syenite breccia at Mont St. Hilaire, Quebec (Grice et al., 1987).

In peraluminous rare-element pegmatites, milarite is locally generated as an alteration product of beryl. This mode of occurrence is well documented in the quartz oligoclasite at Věžná, Czechoslovakia (Černý, 1963, 1968), where milarite is associated with bavenite and cerolite. Much less information is available on one of the two generations of milarite recognized at Radkovice, Czechoslovakia (Černý, 1967), but it also seems to be generated by alteration of beryl. No obvious relationship with altered beryl was reported from Tittling, Bavaria (Tennyson, 1960), or from the Kola peninsula, USSR (Sosedko, 1960), although pseudomorphs after beryl have been recognized at both localities. At Tittling, milarite is associated with albite, muscovite, and zeolites; in the Kola pegmatite, milarite occurs on microcline and albite and is, in turn, overgrown by chabazite and bavenite.

Another mineral for which milarite is a breakdown product is beryllian cordierite ($Al^{3+} + \square \leftarrow Be^{2+} + Na^{+}$; Černý and Povondra, 1966). This alteration also produces abundant celadonite and minor bavenite in the Věžná complex pegmatite (Černý, 1960, 1968), but no associated minerals are evident in this generation of milarite at Radkovice (Černý, 1967). At Maršíkov, Czechoslovakia, milarite crystallizes on schorl within an open fracture in a minor offshoot of the main pegmatite, accompanied by bertrandite and adularia (Staněk, 1964); this occurrence seems to be unrelated to alteration of any primary Be-rich minerals. In contrast, alteration of abundant beryl could have contributed to the crystallization of milarite in the Jaguaraçú pegmatite, Minas Gerais, Brazil, although no direct spatial relationship is apparent. Yttrian milarite is found here in an alpinelike replacement unit, coating albite in association with adularia, late albite, hematite rosettes, muscovite, and quartz, and locally with muscovite, quartz, and acicular tourmaline; minasgeraisite is a late phase covering the milarite crystals (Foord et al., 1986). The paragenetic relationships of milarite in the amazonite pegmatite at Rössing, Namibia, are not known (von Knorring, 1973).

Occurrences of milarite in hydrothermal vein deposits are rather uncommon. In east Siberia, milarite is an alteration product of phenacite and bertrandite, both primary phases of the main Be-CaF_2 mineralization. The milarite formed during later sulphide-carbonate alteration. It has bastnaesite inclusions, grows on albite and calcite, and is subsequently altered to calcite or opal + chalcedony pseudomorphs (Novikova, 1972). In central Asia (Iovcheva et al., 1966), phenacite-bearing albite veins with fluorite, sulfides, epidote, tourmaline, cassiterite, calcite, prehnite, and bavenite have milarite as a late mineral. Its crystallization was accompanied by recrystallization of adjacent phenacite, fluorite, and potassium feldspar, the latter being transformed into adularia. In the epithermal Ag-Au deposit of the Valencia mine, Guanajuato, Mexico (Jensen and Bateman, 1981), milarite crystallized with adularia and quartz and is overgrown by calcite; fluorite, barite, and zeolites are also present in subordinate quantities. Low-temperature veins at Henneberg, Thuringia (Heide, 1953), have milarite in association with barite, fluorite, chalcopyrite, calcite, and minor beryl, bertrandite, and bavenite. All of these four diverse occurrences have a common denominator, a genetic connection with subalkaline leucogranites, or in the case of Guanajuato, A-type rhyolites of related composition (Burt and Sheridan, 1988).

In contrast to the apparent low frequency of milarite in mineralized hydrothermal ore deposits, milarite is widespread in the alpine mineral veins of Switzerland and Austria. This is the type environment of milarite, one that is represented by a large number of localities. They have been extensively reviewed by Parker (1954, 1973) and Hügi and Rowe (1970) for Switzerland and by Niedermayr (1978, 1979) for Austria. In general, milarite-bearing veins are formed in syenitic, granitic, and aplitic rocks. Milarite is associated mainly with quartz, adularia, and chlorite; associations with apatite and fluorite are less common, and those with smoky quartz, hematite,

albite, calcite, actinolitic asbestos, and monazite are rare. In addition, replacement or alteration features are not observed.

General synthesis

This brief review of important localities clearly indicates that there are four principal types of milarite paragenesis. It is less conclusive in terms of specific paragenetic relationships, as these are usually insufficiently described. Nevertheless, the broader mineral associations are fairly well characterized, and it is possible to draw some general conclusions about the circumstances and conditions of milarite crystallization:

1. Milarite is a low-temperature mineral of hydrothermal origin. The composition of the associated adularia (Černý and Chapman, 1984, 1986) and typical crystallization conditions of other associated minerals suggest that milarite crystallizes at temperatures below 300 °C.

2. Milarite is a low-pressure mineral, typically found in vugs of shallow-seated alkaline intrusions or their interior pegmatites, in mesothermal and epithermal ore deposits, and in cavities in alpine veins. Rare-element pegmatites seem to be an exception, as the characteristic pressure range of crystallization is 4–2 kbar (London, 1986). However, subsolidus processes at <300 °C can take place long after thermal equilibration of the pegmatites with their host rocks (usually of lower amphibolite or, rarely, upper greenschist facies) during incipient erosion and regional uplift of the host terrane (London, 1986). Under these circumstances, pressures below 2 kbar are to be expected.

3. The composition of milarite, an alumino-beryllosilicate of K, Na, and Ca, and the nature of its common associates such as adularia, albite, calcite, fluorite, chlorites, and zeolites strongly suggest that milarite crystallizes from alkaline fluids. Other beryllo-silicates and alumino-beryllo-silicates (such as bavenite or epididymite-eudidymite) tend to be contemporaneous with milarite, whereas silicates of Be that are indicative of a low-pH environment (euclase, phenacite, bertrandite) precede or follow the crystallization of milarite (Černý, 1968, 1970).

4. Fluorite and calcite are among the most persistent associates of milarite in all environments (although they are not common in milarite-bearing alpine veins). This supports the suggestions of Beus (1960) that fluor-complexes and carbonate complexes could have been involved in the transportation of Be in the fluid phase.

5. Y is a typical minor-to-substantial component in milarite (Černý et al., 1991). Y and HREE are also complexed and mobile in F- and CO_3-rich fluids (Taylor and Fryer, 1983).

6. In contrast to the above conclusions, there seems to be no simple relationship between parent environment and the extent of the principal $Be^{2+} + Na^{+} \rightleftharpoons Al^{3+} + \square$ substitution in milarite (Černý et al., 1980). The Be content of milarite is evidently governed by such factors as the activities of its principal components and the number and nature of the coprecipitating phases that compete for the relevant cations.

Paragenesis of other members of the milarite group

Some minerals of the milarite group are low-temperature, low-pressure phases as is milarite itself. However, the compositional flexibility of the basic structural framework is reflected in the broad variety of environments hosting other milarite-type minerals, in many cases resulting in stabilization in very diverse *P-T* regimes.

Most of the minerals listed in Table 7 occur in peralkaline rocks: darapiosite, sogdianite, sugilite, eifelite, poudretteite, roedderite, and the closely related species tuhualite, zektzerite, and emeleusite. Host rocks range from protomagmatic assemblages in plutonic intrusions (sugilite and emeleusite at their type localities; Murakami et al., 1976; Upton et al., 1978) through pegmatitic assemblages (sogdianite and darapiosite; Dusmatov et al., 1968; Semenov et al., 1975) and miarolitic pegmatites within parent intrusions (zektzerite and sogdianite; Dunn et al., 1977; Boggs, 1986) to melt-coated cavities in gneissic xenoliths ejected in leucite-tephrite lavas (roedderite and eifelite; Hentschel et al., 1980; Abraham et al., 1983). Poudretteite is found in marble xenoliths within a nepheline-syenite breccia (Grice et al., 1987). The only exception from the overall magmatic affiliation is the African occurrence of sugilite in an obviously metamorphosed manganese ore deposit (Wessels mine, Kalahari; Dunn et al., 1980). However, close association with acmite indicates an alkaline environment analogous to those of the igneous occurrences.

In accord with their affiliation to peralkaline magmas, all of the above minerals are Al poor to Al free, and most have (K,Na) from 2 to 4 apfu. Sugilite is the only exception with 1 (K,Na) pfu, corresponding to the ideal milarite formula. Heterovalent substitutions involving Li, Mg, Fe, Zn, Mn, Zr, and Ti compensate for the Al, except in the case of homovalent B cations in poudretteite. The presence of Li in darapiosite, sogdianite, sugilite (and zektzerite) should also be emphasized: low concentrations of Li in peralkaline igneous suites commonly find their mineralogical expression only in pegmatitic stages (e.g., protolithionite) to which most occurrences of these four minerals are related. The pressure of crystallization ranges from epizonal plutonic to extrusive volcanic, and early magmatic to late-stage pegmatitic temperatures can be assumed.

Another well-defined genetic group consists of three rare minerals from meteorites: yagiite in a small silicate inclusion in an iron meteorite, merrihueite as inclusions in clinopyroxenes, and roedderite (besides its only terrestrial occurrence mentioned above) in enstatite chondrites and octahedrites (Dodd et al., 1965; Fuchs et al., 1966; Bunch and Fuchs, 1969). All three minerals are Al poor to Al free with 1 (K,Na) pfu and are distinctly rich in Mg and Fe. No specific data are available for the conditions of crystallization, although the frequent association with

tridymite may be significant for estimates of minimum temperature of formation. Experimental work indicates very extensive stability fields in the anhydrous systems relevant to most meteorites (stable to ~1100 °C and ~32 kbar; Seifert and Schreyer, 1969). This would explain the occurrences of these minerals in the broad range of meteorite categories mentioned above, from those solidified from high-temperature melts at high pressures (such as octahedrites) to probable low-temperature condensates (chondrites).

The remaining minerals are decidedly individual in their modes of occurrence, a feature that seems dictated primarily by geochemical considerations.

Armenite requires Ba-rich environments. These can be provided by hydrothermal Ag-bearing sulfide mineralization (Neumann, 1941), hydrothermal veins in altered diorite (Pouliot et al., 1984), hydrothermal alteration of granitoid and volcano-sedimentary rocks (Semenenko et al., 1987), and hydrothermal veining of chemical or volcaniclastic sediments hosting metamorphosed sulfide deposits (Balassone et al., 1989; Žák and Obst, 1989). In two of the above occurrences, the temperature of armenite crystallization was estimated as less than 400–300 °C. The only exception to this low-temperature environment seems to be the gneiss-like celsian-rich assemblages from Broken Hill (Mason, 1987).

Brannockite is known only from its type locality, the Foote mine spodumene pegmatites at Kings Mountain, North Carolina (White et al., 1973). It is found in vugs and open fissures with bavenite, tetrawickmannite, pyrite, stannian titanite, albite, and quartz, an assemblage of apparent low-temperature hydrothermal origin. The presence of considerable Li in this mineral is not surprising in view of the spodumene-rich wall rocks; however, Al was evidently not mobilized in significant quantities by the low-temperature fluids, despite the peraluminous environment.

Last but certainly not least, osumilite deserves a special note because of its (Mg,Fe)-rich peraluminous composition, considerable range of composition, and the wide variety of its occurrences. On the one hand, it occurs both as anhedral phenocrysts in the groundmass and as cavity-lining crystals associated with tridymite and quartz in acid volcanic rocks (Miyashiro, 1956; Rossi, 1963; Olsen and Bunch, 1970; Stankevich, 1974; de Michele, 1974; Yokomizo and Miyachi, 1978; Hochleitner, 1982; Schreyer et al., 1983; Parodi et al., 1989) and in buchites (Chinner and Dixon, 1973; Schreyer et al., 1986; Armbruster and Oberhänsli, 1988a). On the other hand, several localities have recently been identified in high-grade metamorphic rocks (Berg and Wheeler, 1976; Maijer et al., 1977; Hensen, 1977; Bogdanova et al., 1980; Ellis, 1980; Ellis et al., 1980; Grew, 1982; Arima and Gower, 1987). Thus the conditions of crystallization range from near-solidus volcanic to granulite-facies metamorphic.

The stability of osumilite was a contentious problem until the early 1980s, as initial attempts at synthesis gave results seemingly irreconcilable with natural occurrences (Euler and Hellner, 1957; Schreyer and Seifert, 1967). This led the latter authors to conclude that metamorphic osumilite might be metastable. It was the more recent work of Hensen (1977) and Olesch and Seifert (1981) in conjunction with petrological studies (Berg and Wheeler, 1976; Ellis, 1980; Grew, 1982; Arima and Gower, 1987) that established the stability of osumilite in both types of environments. Osumilite is stable under near-to-total anhydrous conditions of relatively high-temperature granulite facies metamorphism (>750 °C, P_{tot} < 8–9 kbar; Grew, 1982) and in hydrous magmas at <1 kbar (Olesch and Seifert, 1981). Thus the stability fields of osumilite resemble those of roedderite-merrihueite (Seifert and Schreyer, 1969). Experimental evidence (Schreyer and Seifert, 1967; Olesch and Seifert, 1981) and natural occurrences (Olsen and Bunch, 1970; de Michele, 1974; Berg and Wheeler, 1976; Armbruster and Oberhänsli, 1988a, 1988b) indicate that osumilite is not stable in hydrous low-temperature conditions. The breakdown products seem to be similar to those generated at the expense of cordierite in comparable retrogressive environments.

Summary

Milarite is the prototype mineral for a large structural group of tetrahedral framework minerals involving a wide variety of other tetrahedrally coordinated cations in addition to Si^{4+}. The following points are of importance:

1. The general formula for this structure type can be written as $^{[6]}A_2{}^{[9]}B_2{}^{[12]}C^{[18]}D[^{[4]}T2_3{}^{[4]}T1_{12}O_{30}]$ where A = Al, Fe^{3+}, Sn^{4+}, Mg, Zr, Fe^{2+}, Ca, Na, (Y, REE); B = Na, H_2O, □, Ca(?), K(?); C = K, Na, □, Ca(?); D = □; T1 = Si, Al; and T2 = Li, Be, B, Mg, Al, Si, Mn^{2+}, Zn.

2. The general formula of milarite can be written as $(K,Na)_xK(Ca,Y,REE)_2(Be,Al)_3Si_{12}O_{30}(H_2O)_z$.

3. The important substitutions in milarite are $^{B}Na + {}^{T2}Be \rightleftharpoons {}^{B}\square + {}^{T2}Al$ and $^{A}(Y,REE) + {}^{T2}Be \rightleftharpoons {}^{A}Ca + {}^{T2}Al$. The first is more common, but the second can be significant in REE-enriched environments, and a REE species seems possible.

4. H_2O is always present in milarite and armenite; it is rarely (if ever) present in other species of this group.

5. The ⟨T2-O⟩ distance is linearly dependent on the Be/(Be + Al) ratio, supporting the structure refinement results that indicate direct Be ⇌ Al substitution at the T2 site.

6. In milarite, the A cation (Ca,Y,REE) always shows positional disorder about the central position, even when the site is completely occupied by Ca. The observed average separation is a function of the Be/(Be + Al) ratio.

7. In milarite, the B site is occupied by (H_2O,Na,K) and shows positional disorder that is a function of the Be/(Be + Al) ratio.

8. In milarite, the C site is completely occupied by K, and there is no positional disorder at this site.

9. In the minerals of the milarite group, there is Al ⇌ Si substitution at T1 and a wide variety of substitutions at T2. The sizes of the coordination polyhedra are linearly related to the ionic radii of the constituent cations.

10. There are four principal types of milarite paragenesis: (a) postorogenic and anorogenic intrusions of alkaline affinity, together with their interior pegmatites, (b) peraluminous rare-element pegmatites, (c) hydrothermal vein deposits, and (d) alpine-type veins.

11. Milarite is a low-temperature (<300 °C), low-pressure (usually <2 kbar) mineral of hydrothermal origin.

12. Milarite occurs in alkaline environments, and its persistent association with fluorite and calcite suggests that fluoro- and carbonate complexes were involved in the transport of Be.

13. Y and REE can be significant components in milarite.

14. For the milarite-group minerals, the compositional flexibility of the basic structural framework is reflected in the broad variety of environments hosting these minerals. There are four principal parageneses: (a) Most minerals occur in peralkaline rocks, ranging from protomagmatic assemblages in plutonic rocks through various classes of pegmatites to xenolithic assemblages. (b) A small group (yagiite, merrihueite, roedderite) occurs in meteorites. (c) The occurrence of a small group of very unusual composition (e.g., armenite, brannockite) is dictated by geochemical factors. (d) Osumilite shows a wide range of occurrences in both acid volcanics and in high-grade metamorphic rocks. Given the appropriate bulk composition, a great diversity of conditions can give rise to the crystallization of minerals with the milarite structure. New species have recently been found at a considerable rate, and increasing interest in alkaline rocks has shown the importance of these minerals not only as accessory phases but also as rock-forming minerals.

Acknowledgments

We would like to thank J.L. Jambor (CANMET, Ottawa) for the Strange Lake sample, R.V. Gaines for the Jaguaraçú samples, and John S. White for the samples from the NMNH–Smithsonian Institution (Washington). W.W. Gould assisted with the early stages of the spectroscopic work. Financial assistance was provided by the Natural Sciences and Engineering Research Council of Canada (operating grants to F.C.H. and P.Č.; a major equipment grant, a University Research Fellowship, and an Infrastructure grant to F.C.H.; and a major installation grant to P.Č.) and the NSF grant EAR-8618200 to G.R.R.

References cited

Abraham, K., Gebert, W., Medenbach, O., Schreyer, W., and Hentschel, G. (1983) Eifelite, $KNa_3Mg_4Si_{12}O_{30}$, a new mineral of the osumilite group with octahedral sodium. Contributions to Mineralogy and Petrology, 82, 252–258.

Arima, M., and Gower, C.F. (1987) Osumilite-bearing metasedimentary gneiss in the Grenville Province, eastern Labrador. Geological Association of Canada/Mineralogical Association of Canada Annual Meeting, Saskatoon, Program and Abstracts, 12, 22.

Armbruster, Th. (1989) Crystal chemistry of double-ring silicates: Structure of roedderite at 100 and 300 K. European Journal of Mineralogy, 1, 715–718.

Armbruster, Th., and Oberhänsli, R. (1988a) Crystal chemistry of double-ring silicates: Structural, chemical and optical variation in osumilites. American Mineralogist, 73, 585–593.

——— (1988b) Crystal chemistry of double-ring silicates: Structures of sugilite and brannockite. American Mineralogist, 73, 594–600.

Armbruster, Th., Bermanec, V., Wenger, M., and Oberhänsli, R. (1989) Crystal chemistry of double-ring silicates: Structure of natural and dehydrated milarite at 100 K. European Journal of Mineralogy, 1, 353–362.

Bakakin, V.V., Balko, V.P., and Solovyeva, L.P. (1975) Crystal structures of milarite, armenite, and sogdianite. Soviet Physics Crystallography, 19, 460–462.

Balassone, G., Boni, M., Di Maio, G., and Franco, E. (1989) Armenite in southwest Sardinia: First recorded occurrence in Italy. Neues Jahrbuch für Mineralogie Monatshefte, 1989, 49–58.

Berg, J.H., and Wheeler, E.P. (1976) Osumilite of deep-seated origin in the contact aureole of the Nain complex, Labrador. American Mineralogist, 61, 29–37.

Beus, A.A. (1960) Geochemistry of beryllium and genetic types of beryllium deposits. Akademia Nauk SSSR, Moscow (in Russian).

Bissert, G., and Liebau, F. (1987) Crystal structure of $[N(n\text{-}C_4H_9)_4]H_7[Si_8O_{20}]\cdot 5.33H_2O$—a zeolite A-like double-ring silicate with protonated water clusters $[H_{41}O_{16}]^{9+}$. Zeitschrift für Kristallographie, 179, 357–371.

Bogdanova, N.G., Troneva, N.V., Zaborovskaya, N.B., Sukhanov, M.K., and Berkhin, S.I. (1980) The first find of metamorphic osumilite in the USSR. Doklady Akademia Nauk SSSR, 250, 690–693 (in Russian).

Boggs, R.C. (1986) Miarolitic cavity and pegmatite mineralogy of Eocene anorogenic granite plutons in the northwestern U.S.A. Fourteenth General Meeting, Abstracts with Programs, 58. International Mineralogical Association, Stanford.

Brown, G.E., Jr., and Gibbs, G.V. (1969) Refinement of the crystal structure of osumilite. American Mineralogist, 54, 101–116.

Bunch, T.E., and Fuchs, L.H. (1969) Yagiite, a new sodium-magnesium analogue of osumilite. American Mineralogist, 54, 14–18.

Burt, D., and Sheridan, M. (1988) Mineralization associated with topaz rhyolites and related rocks in Mexico. In R.P. Taylor and D.F. Strong, Eds., Canadian Institute of Mining and Metallurgy Recent advances in the geology of granite-related mineral deposits, 39, 303–306.

Černý, P. (1960) Milarite and wellsite from Věžná. Prace Brnen Zakladny Csav, 32, 1–14.

——— (1963) Epididymite and milarite-alteration products of beryl from Věžná, Czechoslovakia. Mineralogical Magazine, 33, 450–457.

——— (1967) Notes on the mineralogy of some West-Moravian pegmatites. Časopis pro Mineralogii a Geologii, 12, 461–463 (in Czech).

——— (1968) Berylliumminerale in Pegmatiten von Věžná und ihre Umwandlungen. Berichte der Deutschen Gesellschaft für Geologische Wissenschaften, B13, 565–578.

——— (1970) Review of some secondary hypogene parageneses after early pegmatite minerals. Freiberger Forschungshefte C270, Mineralogie und Lagerstättenlehre, 47–67.

Černý, P., and Chapman, R. (1984) Paragenesis, chemistry and structural state of adularia from granitic pegmatites. Bulletin de Minéralogie, 107, 369–384.

——— (1986) Adularia from hydrothermal vein deposits: Extremes in structural state. Canadian Mineralogist, 24, 717–728.

Černý, P., and Povondra, P. (1966) Beryllian cordierite from Věžná: (Na, K) + Be → Al. Neues Jahrbuch für Mineralogie Monatshefte, 1966, 36–44.

Černý, P., Hawthorne, F.C., and Jarosewich, E. (1980) Crystal chemistry of milarite. Canadian Mineralogist, 18, 41–57.

Černý, P., Hawthorne, F.C., Jambor, J.L., and Grice, J.D. (1991) Yttrian milarite. Canadian Mineralogist, in press.

Chinner, G.A., and Dixon, P.D. (1973) Irish osumilite. Mineralogical Magazine, 39, 189–192.

Chistyakova, M.B., Osolodkina, G.A., and Razmanova, Z.P. (1964) Milarite from Central Kazakhstan. Doklady Akademia Nauk SSSR, 159, 1305–1308 (in Russian).

de Michele, V. (1974) Qualche osservazione paragenetica sull'osumilite del Monte Arci (Cagliari). Natura, 64, 39–45.

Dodd, R.T., van Schmus, W.R., and Marvin, U.B. (1965) Merrihueite, a new alkaliferro-magnesian silicate from the Mezo-Madaras chondrite. Science, 149, 972–974.

Dunn, P.J., Rouse, R.C., Cannon, B., and Nelen, J. (1977) Zektzerite: A new lithium sodium zirconium silicate related to tuhualite and the osumilite group. American Mineralogist, 62, 416–420.

Dunn, P.J., Brummer, J., and Belsky, H. (1980) Sugilite, a second occurrence: Wessels mine, Kalahari manganese field, Republic of South Africa. Canadian Mineralogist, 18, 37–39.

Dusmatov, V.D., Efimova, A.F., Kataeva, Z.T., Khoroshilova, L.A., and Yanulov, K.P. (1968) Sogdianite, a new mineral. Doklady Akademia Nauk SSSR, 182, 1176–1177 (in Russian).

Ellis, D.J. (1980) Osumilite-sapphirine-quartz granulites from Enderby Land, Antarctica: P-T conditions of metamorphism, implications for garnet-cordierite equilibria and the evolution of the deep crust. Contributions to Mineralogy and Petrology, 74, 201–210.

Ellis, D.J., Sheraton, J.W., England, R.N., and Dallwitz, W.B. (1980) Osumilite-sapphirine-quartz granulites from Enderby Land, Antarctica—mineral assemblages and reactions. Contributions to Mineralogy and Petrology, 72, 123–143.

Euler, R., and Hellner, E. (1957) Hydrothermale and roentgenographische Untersuchungen an gesteinbildenden Mineralen—V. Uber hydrothermal hergestellten Osumilith. Geochimica et Cosmochimica Acta, 15, 156–157.

Foord, E.E., Gaines, R.V., Crock, J.G., Simmons, W.B., Jr., and Barbosa, C.P. (1986) Minasgeraisite, a new member of the gadolinite group from Minais Gerais, Brazil. American Mineralogist, 71, 603–607.

Forbes, W.C., Baur, W.H., and Khan, A.A. (1972) Crystal chemistry of milarite-type minerals. American Mineralogist, 57, 463–472.

Fuchs, L.H., Frondel, C., and Klein, C., Jr. (1966) Roedderite, a new mineral from the Indarch meteorite. American Mineralogist, 51, 949–955.

Ghose, S., and Wan, C. (1978) Zektzerite, $NaLiZrSi_6O_{15}$: A silicate with six-tetrahedral-repeat double chains. American Mineralogist, 63, 304–310.

Goldman, D.S., and Rossman, G.R. (1978) The site distribution of iron and anomalous biaxiality in osumilite. American Mineralogist, 63, 490–498.

Goldman, D.S., Rossman, G.R., and Dollase, W.A. (1977) Channel constituents in cordierite. American Mineralogist, 62, 1144–1157.

Grew, E.S. (1982) Osumilite in the sapphirine-quartz terrane of Enderby Land, Antarctica: Implications for osumilite petrogenesis in granulite facies. American Mineralogist, 67, 762–787.

Grice, J.D., Ercit, T.S., Van Velthuizen, J., and Dunn, P.J. (1987) Poudretteite $KNa_2B_3Si_{12}O_{30}$, a new member of the osumilite group from Mont Saint-Hilaire, Quebec, and its crystal structure. Canadian Mineralogist, 25, 763–766.

Hawthorne, F.C. (1985) Schneiderhöhnite, $Fe^{2+}Fe^{3+}{}_3As^{3+}{}_5O_{13}$, a densely packed arsenite structure. Canadian Mineralogist, 23, 675–679.

Hawthorne, F.C., and Černý, P. (1977) The alkali metal positions in Cs-Li beryl. Canadian Mineralogist, 15, 414–421.

Hawthorne, F.C., and Smith, J.V. (1986) Enumeration of 4-connected 3-dimensional nets and classification of framework silicates. 3D nets based on insertion of 2-connected vertices into 3-connected plane nets. Zeitschrift für Kristallographie, 175, 15–30.

——— (1988) Enumeration of 4-connected 3-dimensional nets and classification of framework silicates. Combination of zigzag and saw chains with 6^3, 3.12^2, 4.8^2 and $(5^2.8)_2(5.8^2)_1$. Zeitschrift für Kristallographie, 183, 213–231.

Heide, F. (1953) Berylliummineralien vom Heimeberg bei Wurzbade in Thuringen. Chemie der Erde, 16, 33–34.

Hensen, B.J. (1977) The stability of osumilite in high grade metamorphic rocks. Contributions to Mineralogy and Petrology, 64, 197–204.

Hentschel, G., Abraham, K., and Schreyer, W. (1980) First terrestrial occurrence of roedderite in volcanic ejecta of the Eifel, Germany. Contributions to Mineralogy and Petrology, 73, 127–130.

Hesse, K.-F. and Seifert, F. (1982) Site occupancy refinement of osumilite. Zeitschrift für Kristallographie, 160, 179–186.

Hochleitner, R. (1982) Osumilith: Osumilith-Kristalle von der Lava Funtanafigu. Lapis, 7(11), 26–27.

Hügi, T., and Rowe, D. (1970) Berylliummineralien und Berylliumgehalte granitischer Gesteine der Alpen. Schweizerische Mineralogische Petrographische Mitteilungen, 50, 477–480.

International tables for X-ray crystallography, vol. IV (1974) Kynoch Press, Birmingham, England.

Iovcheva, E.I., Kupriyanova, I.I., and Sidorenko, G.A. (1966) Milarite from central Asia. Doklady Akademia Nauk SSSR, 170, 1394–1397 (in Russian).

Janeczek, J. (1986) Chemistry, optics, and crystal growth of milarite from Strzegom, Poland. Mineralogical Magazine, 50, 271–277.

Jensen, M.L., and Bateman, A.M. (1981) Economic mineral deposits. Wiley, New York.

Kato, T., Miura, Y., and Murakami, N. (1976) Crystal structure of sugilite. Mineralogical Journal, 8, 184–192.

Khan, A.A., Baur, W.H., and Forbes, W.C. (1971) Synthetic magnesium merrihueite, a dipotassium pentamagnesium dodecasilicate: A tetrahedral magnesiosilicate framework crystal structure. Acta Crystallographica, B28, 267–272.

Kimata, M., and Hawthorne, F.C. (1989) The crystal chemistry of milarite: Two split-site model. Annual Report of the Institute of Geosciences, University of Tsukuba, 15, 92–95.

Kuschel, H. (1877) Mitteilung an Prof. G. Leonhard. Milarit. Neues Jahrbuch für Mineralogie, Geologie und Palaeontologie, 925–926.

Liebau, F. (1985) Structural chemistry of silicates. Springer-Verlag, Berlin.

London, D. (1986) Magmatic-hydrothermal transition in the Tanco rare-element pegmatite: Evidence from fluid inclusions and phase-equilibrium experiments. American Mineralogist, 71, 376–395.

Maijer, C., Hansen, J.B.H., Wevers, J., and Poorter, R.P.E. (1977) Osumilite, a mineral new to Norway. Norsk Geologisk Tidsskrift, 57, 187–188.

Mason, B. (1987) Armenite from Broken Hill, Australia, with comments on calciocelsian and barium anorthite. Mineralogical Magazine, 51, 317–318.

Merlino, S. (1969) Tuhualite crystal structure. Science, 166, 1399–1401.

Miller, G.H., Rossman, G.R., and Harlow, G.E. (1987) The natural occurrence of hydroxide in olivine. Physics and Chemistry of Minerals, 14, 461–472.

Miyashiro, A. (1956) Osumilite, a new silicate mineral and its crystal structure. American Mineralogist, 41, 104–116.

Moore, P.B., and Shen, J. (1983) An X-ray structural study of cacoxenite, a mineral phosphate. Nature, 306, 356–358.

Murakami, N., Kato, T., Miura, Y., and Kirotatari, F. (1976) Sugilite, a new silicate mineral from Iwagi Islet, southwest Japan. Mineralogical Journal (Japan), 8, 110–121.

Neumann, H. (1941) Armenite, a water-bearing barium-calcium-aluminosilicate. Norsk Geologisk Tidsskrift, 21, 19–24.

Niedermayr, G. (1978) Ein ungewohnlicher Milaritfund aus Salzburg, Osterreich. Aufschluss, 29, 355–357.

——— (1979) Neue Funde von Milarit und Bavenit. Aufschluss, 30, 147–149.

Novikova, M.I. (1972) Milarite from Eastern Siberia. Trudy Mineralogicheskogo Musega Akademii Nauk SSSR, 21, 188–192 (in Russian).

Oftedal, I., and Saebö, P.C. (1965) Contributions to the mineralogy of Norway. 30. Minerals from nordmarkite druses. Norsk Geologisk Tidsskrift, 45, 171–175.

Olesch, M., and Seifert, F. (1981) The restricted stability of osumilite under hydrous conditions in the system K_2O-MgO-Al_2O_3-SiO_2-H_2O. Contributions to Mineralogy and Petrology, 76, 362–367.

Olsen, E., and Bunch, T.E. (1970) Comparison of natural osumilites. American Mineralogist, 55, 875–879.

Palache, C. (1931) On the presence of beryllium in milarite. American Mineralogist, 16, 469–470.

Parker, R.L. (1954) Die Mineralfunde der Schweizer Alpen. Wepf and Co. Verlag, Basel, Switzerland.

——— (1973) Die Mineralfunde der Schweizer Alpen. Wepf and Co., Basel, Switzerland.

Parodi, G.C., Della Ventura, G., and Lorand, J.-P. (1989) Mineralogy and petrology of an unusual osumilite + vanadium-rich pseudobrookite assemblage in an ejectum from the Vico volcanic complex (Latium, Italy). American Mineralogist, 74, 1278–1284.

Perrault, G., and Szymanski, J.T. (1982) Steacyite, a new name and a re-evaluation of the nomenclature of "ekanite"-group minerals. Canadian Mineralogist, 20, 59–64.

Pouliot, G., Trudel, P., Valiquette, G., and Samson, P. (1984) Armenite-

thulite-albite veins at Remigny, Quebec: The second occurrence of armenite. Canadian Mineralogist, 22, 453–464.

Pushcharovskii, D.Yu., Baataryn, T., Pobedimskaya, E.A., and Belov, N.V. (1972) The crystal structure of the zinc analogue of milarite. Soviet Physics Crystallography, 16, 628–630.

Raade, G. (1966) A new Norwegian occurrence of milarite. Norsk Geologisk Tidsskrift, 46, 122–123.

Richard, P., and Perrault, G. (1972) La structure cristalline de l'ekanite $Th_{2-x}(Na,Ca)_{4-y}K_{2-z}Si_{16}O_{40}$. Acta Crystallographica, B28, 1994–1999.

Rossi, G. (1963) Ritrovamento della osumilite in una riolite del Monte Arci. Rendiconti di Societa di Mineralogia Italiana, 19, 187–193.

Rossman, G.R. (1975) Joaquinite: The nature of its water content and the question of four-coordinated ferrous iron. American Mineralogist, 60, 435–440.

Sandomirskii, P.A., Simonov, M.A., and Belov, N.V. (1977) Crystal structure of synthetic Mn-milarite $K_2Mn_5[Si_{12}O_{30}]\cdot H_2O$. Soviet Physics Doklady, 22, 181–183.

Schreyer, W., and Seifert, F. (1967) Metastability of an osumilite end member in the system K_2O-MgO-Al_2O_3-SiO_2-H_2O and its possible bearing in the rarity of natural osumilites. Contributions to Mineralogy and Petrology, 14, 343–358.

Schreyer, W., Hentschel, G., and Abrahan, K. (1983) Osumilith in der Eifel und die Verwendung Minerals als petrogenetischer Indikator. Tschermaks Mineralogische und Petrographische Mitteilungen, 32, 215–234.

Schreyer, W., Blumel, P., and Maresch, W. (1986) Cordierit und Osumilith aus den Buchiten der Blauen Kuupe bei Eschwege. Aufschluss, 37, 353–367.

Seifert, F., and Schreyer, W. (1969) Stability relations of $K_2Mg_5Si_{12}O_{30}$, an end member of the merrihueite-roedderite group of meteoritic minerals. Contributions to Mineralogy and Petrology, 22, 190–207.

Semenenko, N.P., Litvin, A.L., Sharkin, O.P., Boiko, V.L., Egorova, L.N., Skuridin, G.S., Terets, G.Ya., Savitskaya, A.B., and Ilovaiskaya, S.V. (1987) Armenite from Northern Dneiper region. Mineralogical Zhurnal, 9, 83–90.

Semenov, E.I., Dusmatov, V.D., Khomyakov, A.P., Voronkov, A.A., and Kazakova, M. (1975) Darapiosite, a new mineral of the milarite group. Zapiski Vsesoyuznogo Mineralogicheskogo Obshchestva, 104, 583–584 (in Russian).

Shannon, R.D. (1976) Revised effective ionic radii and systematic studies of interatomic distances in halides and chalcogenides. Acta Crystallographica, A32, 751–767.

Sheldrick, G. (1981) Nicolet SHELXTL operations manual. Nicolet XRD Corporation, Madison, Wisconsin.

Shoemaker, D.P., Robson, H.E., and Broussard, L. (1973) The "sigma-transformation" interrelating certain known and hypothetical zeolite structures. In J.B. Uytterhoeven, Ed., Molecular sieves, p. 138–143. Leuven University Press, Leuven, Belgium.

Skogby, H., Bell, D.R., and Rossman, G.R. (1990) Hydroxide in pyroxene: Variations in the natural environment. American Mineralogist, 75, 764–774.

Smith, J.V. (1977) Enumeration of 4-connected 3-dimensional nets and classification of framework silicates. I. Perpendicular linkages from simple hexagonal net. American Mineralogist, 62, 703–709.

Sosedko, T.A. (1960) An occurrence of milarite on the Kola Peninsula. Doklady Akademii Nauk SSSR, 131, 643–646 (in Russian).

Staněk, J. (1964) Milarite and triplite from the Maršíkov pegmatite in northern Moravia. Acta Musei Moraviae, 49, 33–38 (in Czech).

Stankevich, Ye.K. (1974) Osumilite from volcanic rocks of the Caucasus. Nauka Leningrad, 60–64 (in Russian).

Taylor, R.P., and Fryer, B.J. (1983) Rare earth element lithogeochemistry of granitoid mineral deposits. Canadian Institute of Mining and Thaumaturgy Bulletin, 76, 74–84.

Tennyson, C. (1960) Berylliummineralien und ihre pegmatitische Paragenese in den Graniten von Tittling/Bayerischer Wald. Neues Jahrbuch für Mineralogie Abhandlungen, 94, 1253–1265.

Upton, B.G.J., Holl, P.G., Johnsen, O., and Petersen, O.V. (1978) Emeleusite: A new $LiNaFe'''$ silicate from south Greenland. Mineralogical Magazine, 42, 31–34.

Velde, D., Medenbach, O., Wagner, C., and Schreyer, W. (1989) Chayesite, $K(Mg,Fe^{2+})_4Fe^{3+}[Si_{12}O_{30}]$: A new rock-forming silicate of the osumilite group from the Moon Canyon (Utah) lamproite. American Mineralogist, 74, 1368–1373.

von Knorring, O. (1973) Notes on pegmatite minerals from Rwanda, Uganda and South West Africa. Seventeenth Annual Report of the Research Institute of African Studies of the University of Leeds, 72–73.

White, J.S., Jr., Arem, J.E., Nelen, J.A., Leavens, P.B., and Thomssen, R.W. (1973) Brannockite, a new tin material. Mineralogical Record, 4, 73–76.

Wood, D.L., and Nassau, K. (1967) Infrared spectra of foreign molecules in beryl. Journal of Chemical Physics, 47, 2220–2228.

Yokomizo, H., and Miyachi, S. (1978) Chemical composition of osumilite in Haneyama lava, Oita Prefecture. Journal of Japanese Association of Mineralogists, Petrologists and Economic Geologists, 73, 180–182 (in Japanese).

Žák, L., and Obst, P. (1989) Armenite-feldspar veins in basic volcanic rocks from Chvaletice (Czechslovakia). Časopis pro Mineralogii a Geologii, 34, 337–351.

Zoltai, T. (1960) Classification of silicates and other minerals with tetrahedral structures. American Mineralogist, 45, 960–973.

Manuscript received October 1, 1990
Manuscript accepted July 13, 1991